Journal of Fluids and Structures 87 (2019) 58–83

Contents lists available at ScienceDirect

Journal of Fluids and Structures

journal homepage: www.elsevier.com/locate/jfs

Linear wave response of a 2D closed flexible fish cage

Ida M. Strand *, Odd M. Faltinsen

Centre for Autonomous Marine Operations and Systems, Department of Marine Technology, Norwegian University of Science and Technology, Trondheim, Norway

HIGHLIGHTS

- A linear model of a floating 2D closed flexible fish cage in waves was developed.
- The flexibility of the cage is significant for the rigid body motion response.
- Large internal wave amplitudes are predicted at the 1. and 3. sloshing frequencies.
- Limitations of model tests of a closed flexible fish cage were shown.

ARTICLE INFO

Article history:
Received 19 January 2018
Received in revised form 31 January 2019
Accepted 12 March 2019
Available online 25 March 2019

Keywords:
Hydroelasticity
Membrane
Aquaculture
Waves
Sloshing

ABSTRACT

Closed flexible fish cages (CFFC) are proposed as a new concept in marine aquaculture, replacing the conventional net cages in order to meet ecological challenges related to fish lice and escapes. A linear mathematical model of a freely floating 2D CFFC in waves have been developed. It was found that the wave induced rigid body motion responses of a flexible CFFC in sway, heave and roll are significantly different from the responses of a rigid CFFC. Large ratios between free-surface elevation amplitudes and incident wave amplitude are predicted inside the tank at the first and third natural sloshing frequencies. It implies that non-linear free surface effects must be accounted for inside the tank in realistic sea conditions. The dynamic tension in the membrane of the CFFC must be smaller than the static tension in the applied structural method. For the analysed case with 25 m between the centre of the floaters, the most probable largest dynamic tension is larger than the static tension, for significant wave heights larger than 0.5 meter. The effect of scaling of elasticity on the rigid body motion have also been investigated. The non-dimensional response of the CFFC versus non-dimensional frequency, and based on Froude scaling using an elasticity available in model scale have been compared to the response of the CFFC using the elasticity for full scale. These responses were found to deviate to a large extent, showing limitations of model tests of a CFFC.

1. Introduction

Norway has become the World's largest producer of Atlantic salmon through the use of open net structures in the sea. The aquaculture facilities have grown in both size and number. Currently, the industry faces increased attention on environmental challenges related to fish escapes, sea lice, diseases, and pollution. A possible solution is to use a Closed Flexible Fish Cage (CFFC). This is a system that consists of a floater, a mooring-system and an impermeable flexible

* Corresponding author.
E-mail address: ida.strand@ntnu.no (I.M. Strand).

https://doi.org/10.1016/j.jfluidstructs.2019.03.005
0889-9746/

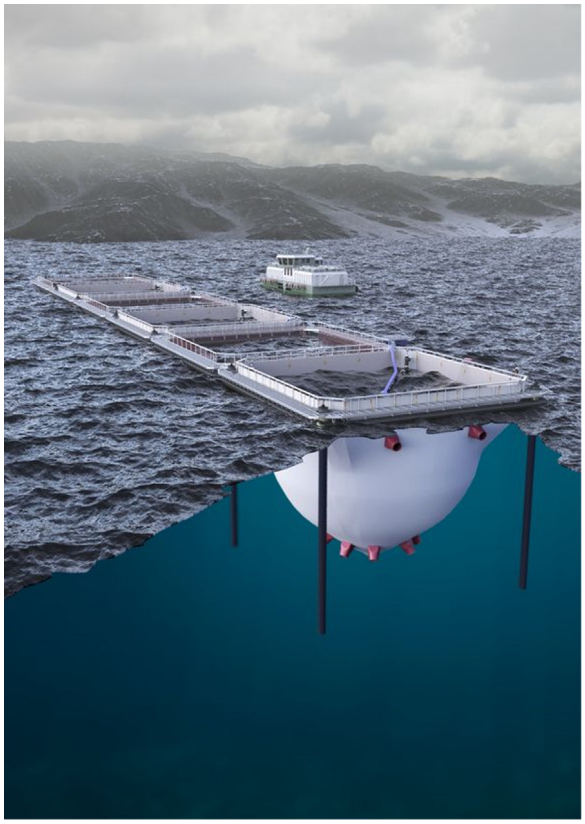

Fig. 1. Illustrative figure of full scale closed flexible fish cage used by Botngaard AS. Courtesy of Botngaard.

membrane replacing the traditional nett, see Fig. 1 for an illustration of a full scale closed flexible fish cage. This membrane is typically made of a light weight fabric material, which is close to neutrally buoyant in water. Compared to a net-based structure the dynamic behaviour of the new membrane-based system changes significantly. One reason is that viscous loads dominate on a net cage in waves and current (Kristiansen and Faltinsen, 2012, 2015), while potential flow loads with body–wave generation is significant for a CFFC in waves. Model experiments for both still water (Strand et al., 2014), current (Lader et al., 2015; Strand et al., 2016) and waves (Lader et al., 2017) have been performed, for various filling levels and geometries. Resonant internal water motion (sloshing) was observed in model tests with a CFFC both by Solaas et al. (1993) and by Lader et al. (2017). All the results showed that the CFFC is flexible, behaves hydro-elastically and that the response is highly dependent on both geometry and filling level.

The deformations and forces on the CFFC depend on both the external and internal hydrodynamic pressure and the structural dynamics. It is crucial to understand the dependency between forces and deformations to develop models, which predict the correct environmental forces and response. Limited scientifically published material is available related to the effect of sea loads on closed flexible fish cages. The dynamics of a real closed flexible fish cage in the sea is clearly three dimensional. However, to develop theory and understanding of the coupling between structural response, and external and internal wave motions we start basic, and the problem is simplified to a 2D problem. A 2D solution will not be representative of the real life cage, but can be used as a starting point to gather knowledge of the behaviour of this structure in waves.

Due to the limited background theory of sea loads on CFFCs, theory for comparable structures is used as background knowledge. A structure resembling the CFFC is the flexible containment bag used for transportation of fresh water or oil, first described by Hawthorne (1961). However, this structure have no internal free surface as the CFFC. For the flexible containment bags, the elasticity of the material and the tension in the fabric govern the shape and flexibility of a fabric structure (Løland and Aarsnes, 1994). The response of the floating liquid-filled fabric structure in waves have been examined and analysed both numerically and experimentally by Zhao and Triantafyllou (1994), Løland and Aarsnes (1994), Zhao (1995) and Phadke and Cheung (2001). Mathematical models of the containment bags have mostly been formulated in 2D. The total pressure on the bag is an interaction between the internal and external pressure forces. All cited references have used linear theory both for the liquid flow and the structural response in their numerical evaluations. However, Zhao and Aarsnes (1998) stated that linear flow theories for flexible containers are only valid for small incident

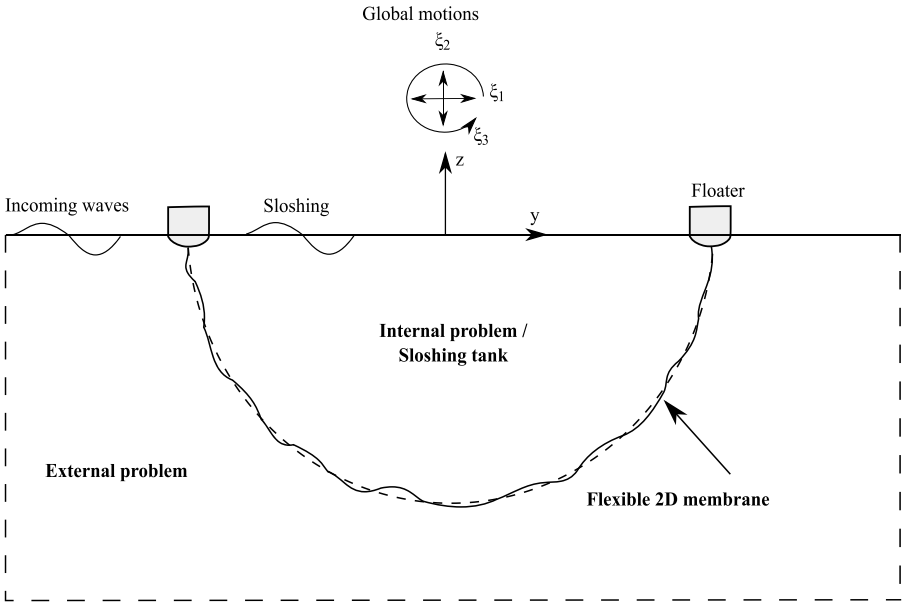

Fig. 2. Illustration of the sub-problems that needs to be solved to predict the response of a 2D CFFC in waves. The dotted line is the equilibrium position of the membrane in calm water.

wave slopes and do not apply for survival wave conditions (Løland and Aarsnes, 1994). One reason is wave over-topping due to small free board.

To predict the response of a 2D CFFC in waves three coupled sub-problems must be solved: the membrane dynamics, the external problem with incident waves and the effect of the structure on the flow, and the internal problem, which is an internal sloshing problem. The floaters are assumed horizontally rigidly connected, and ambient current and internal structures such as pumps and pipes are neglected. Our formulations are based on a linear perturbation about the static mean position of the membrane, and allows for the general case for a static tension variation along the membrane. The stationary geometry and static tension for a given filling level and floater size is needed in the dynamic analysis. For floating large volume offshore structures second order slowly varying and mean wave forces have great importance in the design of the mooring system. These effects will not be considered in the present analysis.

In this paper the linear theory of a 2D CFFC in waves is developed and analysed with the aim to find the response of the CFFC in waves. First a general overview of the problem and the frequency-domain equations of motions of the rigid body motions are presented. The theory for dynamic deformation of a 2D membrane is developed next. Then, the theory for the pressure loads on the CFFC are investigated starting with the external hydrodynamic pressure forces, continuing with internal hydrodynamic pressure forces. The numerical solution of the hydrodynamic problem is outlined, before the total equations for the coupled system is presented. Finally, the results from a 2D case study with relevant full scale dimensions considering a half circularly shaped CFFC with floaters in waves are presented. At last conclusions with future suggested needed investigations are given.

2. Theory for wave induced motions of a closed flexible fish cage

The 2D CFFC consists of two rigidly connected floaters and a membrane (see Fig. 2). An Earth-fixed Cartesian coordinate system Oyz is introduced with origin in the mean free surface. The z-axis pointing upwards is in the centre-plane of the CFFC at rest. The membrane is connected to the floaters at $(\pm R, z_e)$. The static analysis of the 2D membrane has similarities with the analysis of a cable used in a mooring system (Faltinsen, 1990). The important differences are the minor role of the weight and viscous loads and the major role of the hydrostatic pressure for the relevant 2D membrane without ambient current.

The initial shape and tension of the membrane must be known in order to analyse a 2D membrane in waves. The membrane material is sown in a given initial shape, for the analysed case a half circular initial shape is chosen as illustrated in Fig. 2. For the cases examined in Strand et al. (2014), the closed cages were underfilled, and the shape of the cage was dependent on the load history. Overfilled cages are the most plausible from an operational point of view, and this opens for the use of linear theory. To be able to use linear dynamic theory in waves, the sum of static and dynamic membrane tension must be larger than zero. We secure a static tension greater than zero in calm water by introducing a pressure difference over the membrane. This means that there is a positive hydrostatic pressure difference at the membrane between the inside enclosed volume and the surrounding water due to different free surface levels and/or water densities. The shape

of the membrane will then be dependent on this pressure difference. Different internal and external water densities will not be treated in this article, but the equations are developed to allow for more general cases. If the membrane can be assumed massless, the geometry of the membrane below the floaters will remain half circular. A massless membrane can be justified if $m_M g \ll \Delta h \rho_w g ds$, where m_M is the membrane mass per unit area, Δh is the overfilling height, ρ_w is the density of the water and g is the gravity. The initial geometry of the membrane, the static tension T_0, which is a static membrane tension per unit length in the perpendicular x-direction and the vertical submergence of the floaters z_e are known from a static pressure analysis in calm water (Strand, 2018).

The floaters move in waves with the rigid body motions ξ_1, ξ_2 and ξ_3 in sway, heave and roll, respectively. Sway and heave are for a point that coincides with the origin of the coordinate system Oyz when the body is at rest. The motion of the membrane is the sum of the membrane deformations relative to the static shape and rigid body motions described by ξ_1, ξ_2 and ξ_3. It implies that the membrane deformations are zero at the attachment points to the floaters. We assume small rigid body motions of the CFFC and small membrane deformations. Then the superposition principle can be used. The water surrounding and inside the CFFC introduces pressure forces on the combined structure. Potential flow of incompressible water with linear free-surface conditions are assumed. The water has infinite horizontal extent and constant finite water depth.

2.1. Equation of motion

We start by formulating the equations of motions separately for the floaters and the membrane. The equations of rigid body motions follow from Newton's law and the equations of angular momentum. When considering the equations of motions separately for the floater and the membrane, internal loads associated with the rigid-body motions appear at the attachment point between the floater and the membrane. These internal loads can be avoided to be considered by adding the equations of the rigid body motions for the floaters and the membrane and using the principle of action and reaction. However, we must consider loads on the floater caused by the elastic deformations of the membrane. These are expressed as coupled added mass and damping loads caused by the elastic deformations. In addition, the membrane causes dynamic forces at he connection between the floater and the membrane. We must account for both internal and external dynamic loads acting on the floaters and the membrane. The change in hydrostatic loads due to dynamic waves are accounted for in addition to dynamic weight considerations. Assuming steady-state oscillatory conditions, the rigid-body equations of motions of the CFFC becomes:

$$(m_T + a_{11})\ddot{\xi}_1 + b_{11}\dot{\xi}_1 + (a_{13} - z_G m_T)\ddot{\xi}_3 + b_{13}\dot{\xi}_3 = f_1^{exc} + f_1^{Mem}, \tag{1}$$

$$(m_T + a_{22})\ddot{\xi}_2 + b_{22}\dot{\xi}_2 + c_{22}\xi_2 = f_2^{exc} + f_2^{Mem}, \tag{2}$$

$$(I_{33} + a_{33})\ddot{\xi}_3 + b_{33}\dot{\xi}_3 + c_{33}\xi_3 + (a_{31} - z_G m_T)\ddot{\xi}_1 + b_{31}\dot{\xi}_1 = f_3^{exc} + f_3^{Mem}. \tag{3}$$

Here, m_T is the total mass of the floater and membrane per meter, and I_{33} is the combined moment of inertia of the membrane and floaters in roll defined as $I_{33} = \int (y^2 + z^2) dm_T$. a_{jk} are the 2D added mass coefficients associated with the internal and external flow and b_{kj} are the 2D wave radiation damping coefficients. The effect of the membrane deformations on the rigid body motions are given by the forces on the right side of the equation. A general time domain formulation would involve convolution integral formulation of the hydrodynamic loads (Faltinsen, 2005). The considered restoring coefficients c_{jk} in the equation of motions of the floater and the membrane are due to quasi-steady change in the hydrostatic pressure and weight considerations, further described in Section 2.4.1. The effect of a mooring system is not considered. Furthermore, f_j^{exc} and f_j^{Mem} are wave excitation loads on the floater when restrained from oscillating and loads caused by the elastic deformations of the membrane on the floater, respectively. One part of f_j^{Mem} are caused by the flow due to the normal membrane deformations and can be expressed in terms of coupled added mass and damping coefficients. The other part can be represented in terms of restoring coefficients due to membrane forces at the attachment between the membrane and the floater (see Section 2.4.1). How to evaluate a_{jk}, b_{jk} and f_j^{exc} are described in Section 2.5. The membrane deforms as a reaction to the pressure forces, developed equations for the membrane deformations based on Newton's law will now follow.

2.2. Dynamic structural modelling of 2D membrane

We will now solve the dynamic displacement of a 2D membrane with a free surface in the presence of the floater. Bliek (1984) has considered non-linearly a 3D cable in an accelerated coordinate system, which is partly relevant for a 2D membrane. To find the dynamic motions of an infinitesimal element of the 2D membrane the change of tension force along a 2D membrane element must be expressed. The tension in the membrane works along the actual dynamic geometry. Its effect is transferred to the mean static representation in the linear dynamic structural model. The change of tension force along a 2D membrane element of small length ds is $\frac{\partial(T\boldsymbol{t_D})}{\partial s} ds$. The instantaneous tangential ($\boldsymbol{t_D}$) and normal ($\boldsymbol{n_D}$) unit vectors of a membrane element can for small dynamic angles $\hat{\psi}$ be expressed as:

$$\boldsymbol{t_D} = \cos\hat{\psi}\boldsymbol{t} + \sin\hat{\psi}\boldsymbol{n} \approx \boldsymbol{t} + \hat{\psi}\boldsymbol{n}, \tag{4}$$

$$\boldsymbol{n_D} = -\sin\hat{\psi}\boldsymbol{t} + \cos\hat{\psi}\boldsymbol{n} \approx -\hat{\psi}\boldsymbol{t} + \boldsymbol{n}, \tag{5}$$

where $\boldsymbol{n}$, $\boldsymbol{t}$ are the normal and tangential unit vectors respectively, at the mean static position of the membrane, with the normal vector pointing into the CFFC and the tangential vector pointing along the membrane from left to right. It follows that

$$\frac{\partial(T\boldsymbol{t_D})}{\partial s} = \frac{\partial T}{\partial s}\boldsymbol{t_D} + T\frac{\partial \boldsymbol{t_D}}{\partial s} = (\frac{\partial T}{\partial s} - T\frac{\partial \psi}{\partial s}\hat{\psi})\boldsymbol{t} + (T\frac{\partial \psi}{\partial s} + \frac{\partial T}{\partial s}\hat{\psi})\boldsymbol{n}. \tag{6}$$

by using the Frenet formulas (e.g. Kreyszig et al., 2006) as the relation between the normal and tangential vectors $\frac{\partial \boldsymbol{t}_D}{\partial s} = \boldsymbol{n}_D\frac{\partial \psi}{\partial s}$, $\frac{\partial \boldsymbol{n}_D}{\partial s} = -\boldsymbol{t}_D\frac{\partial \psi}{\partial s}$, where ψ is the total angle between the tangent of the membrane and the horizontal plane and T is the tension force per unit length.

By using Newtons second law, Eq. (6) and neglecting structural damping it follows that the dynamic motions of an infinitesimal element of the 2D membrane must satisfy

$$m_M\ddot{v} = T\frac{\partial \psi}{\partial s} + \frac{\partial T}{\partial s}\hat{\psi} - m_M g\cos\psi - \Delta p, \tag{7}$$

$$m_M\ddot{u} = \frac{\partial T}{\partial s} - T\frac{\partial \psi}{\partial s}\hat{\psi} - m_M g\sin\psi. \tag{8}$$

Here, m_M is the membrane mass per unit area, v is the normal displacement of the membrane along $\boldsymbol{n}$, u is the tangential deformation of the membrane along $\boldsymbol{t}$ and Δp is the pressure difference between the internal and external pressure at the membrane. A dot above a variable represents time differentiation. We make a perturbation of the equations about the static solution such that

$$\begin{aligned} \psi(s,t) &= \psi_0(s) + \hat{\psi}(s,t), \\ T(s,t) &= T_0(s) + \tau(s,t) = T_0(s) + Ed\hat{e}(s,t), \\ \Delta p(s,t) &= \Delta p_0 + \Delta\hat{p}(s,t). \end{aligned} \tag{9}$$

Here, $\tau = Ed\hat{e}$ is the dynamic tension where E is the elasticity module, d is the thickness of the membrane and $\hat{e}$ is the dynamic strain following from the linear relation between strain and tension according to Hooke's law. Δp_0 is the static pressure difference and $\Delta\hat{p}$ the dynamic pressure difference. To be able to apply linear theory for the structure, the total tension T of the membrane most be positive, this is because the fabric membrane do not handle compression and will wrinkle when compressed.

After subtracting the static equilibrium equations and keeping linear terms we get:

$$m_M\ddot{v} = T_0\frac{\partial \hat{\psi}}{\partial s} + \tau\frac{\partial \psi_0}{\partial s} + \frac{\partial T_0}{\partial s}\hat{\psi} - m_M g\sin\psi_0\hat{\psi} - \Delta\hat{p}, \tag{10}$$

$$m_M\ddot{u} = \frac{\partial \tau}{\partial s} - T_0\frac{\partial \psi_0}{\partial s}\hat{\psi} - m_M g\cos\psi_0\hat{\psi}. \tag{11}$$

Linear compatibility relations between the deformations (u, v), the dynamic strain $\hat{e}$ and the dynamic angle $\hat{\psi}$ exists (e.g. Ventsel, 2001). By assuming steady state oscillations we find

$$\hat{e} = \frac{\partial u}{\partial s} - v\frac{\partial \psi_0}{\partial s}, \tag{12}$$

$$\hat{\psi} = \frac{\partial v}{\partial s} + u\frac{\partial \psi_0}{\partial s}. \tag{13}$$

Eqs. (12) and (13) show that finite curvature of the static membrane configuration causes coupling between u and v. Since we assume steady state oscillations, we write $u(\psi,t) = u(\psi)e^{i\omega t}$ and $v(\psi,t) = v(\psi)e^{i\omega t}$, where $i^2 = -1$. It implies that $u(\psi,t)$ and $v(\psi,t)$ are complex variables and that it is the real part of $u(\psi,t)\exp(i\omega t)$ and $v(\psi,t)\exp(i\omega t)$ that have physical meaning. Eq. (13) is used in (10) and (11), with the resulting equation system for the normal and tangential deformations:

$$\begin{aligned} -\omega^2 m_M v =& T_0\left(\frac{\partial^2 v}{\partial s^2} + \frac{\partial u}{\partial s}\frac{\partial \psi_0}{\partial s} + u\frac{\partial^2 \psi_0}{\partial s^2}\right) + Ed\left(\frac{\partial u}{\partial s} - v\frac{\partial \psi_0}{\partial s}\right)\frac{\partial \psi_0}{\partial s} + \frac{\partial T_0}{\partial s}\left(\frac{\partial v}{\partial s} + u\frac{\partial \psi_0}{\partial s}\right) \\ & - m_M g\sin\psi_0\left(\frac{\partial v}{\partial s} + u\frac{\partial \psi_0}{\partial s}\right) - \Delta\hat{p}, \end{aligned} \tag{14}$$

$$-\omega^2 m_M u = Ed\left(\frac{\partial^2 u}{\partial s^2} - \frac{\partial v}{\partial s}\frac{\partial \psi_0}{\partial s} - v\frac{\partial^2 \psi_0}{\partial s^2}\right) - T_0\frac{\partial \psi_0}{\partial s}\left(\frac{\partial v}{\partial s} + u\frac{\partial \psi_0}{\partial s}\right) - m_M g\cos\psi_0\left(\frac{\partial v}{\partial s} + u\frac{\partial \psi_0}{\partial s}\right). \tag{15}$$

The hydrodynamic pressure difference $\Delta\hat{p}$ in (14) depends on v, the rigid body motions as well as the incident waves and its diffraction (scattering) by the CFFC. Details are given in Section 2.5. If the static geometry of the membrane is semi circular, (14) and (15) can be simplified to a large extent. The equations for a semi-circular membrane are given in B.

2.3. Coupled system equations for the CFFC

We will solve (14) and (15) by a modal method. That means we write

$$v = \Re\Big(\sum_{m=4}^{\infty} \xi_m U_{(m-3)}(\psi_0) e^{\mathrm{i}\omega t}\Big), \tag{16}$$

$$u = \Re\Big(\sum_{n=1}^{\infty} \mu_n U_n(\psi_0) e^{\mathrm{i}\omega t}\Big), \tag{17}$$

where $\Re$ means the real part and ξ_m for $m > 3$ and μ_n are the generalised complex structural mode amplitudes in normal and tangential direction, respectively. In the following text we will omit the symbol $\Re$ and imply implicitly that we mean the real part of a complex expression involving the complex time dependence. The modal representation must be complete in a mathematical sense. A complete Fourier series (modal) representations of v and u that satisfy the condition of rigid attachment at the floater are chosen as:

$$U_j(\psi_0) = \sin\left(\frac{\pi j(\psi_0 - \psi_e)}{2\psi_e}\right). \tag{18}$$

Here ψ_e are the attachment angle between the membrane and the right floater as illustrated Fig. 3. The modal representation assumes right–left symmetry of the static geometry.

The rigid body equation of motion given by (1)–(3) and the equations for the structural deformations of the membrane by (14) and (15) combined with (16) and (17), multiplied with the mode and integrated along the membrane, together give a representation of the dynamics of the CFFC. In $\boldsymbol{\xi}$ the first three terms are the rigid body motions, then the normal structural deformation modes follows. The membrane influences the rigid body motion through the hydrodynamic coupling terms between rigid body motions and the structural normal deformation modes, and through the connection forces on the floater from dynamic tension and dynamic angle.

When reformulating the equations for the membrane, we substitute Eqs. (16) and (17) into the equations, multiply with (18) and integrate along the membrane length S_M. The coupled equation system can be expressed as:

$$\sum_{j=1}^{\infty}\left(-\omega^2(m_{ij}^{\xi} + a_{ij}) + \mathrm{i}\omega b_{ij} + c_{ij} + c_{ij}^{M\xi}\right)\xi_j + \sum_{n=1}^{\infty} c_{in}^{M\xi\mu}\mu_n = f_i^{exc} \text{ for } i = 1....\infty \tag{19}$$

$$\sum_{j=1}^{\infty} c_{kj}^{M\mu\xi}\xi_n + \sum_{n=1}^{\infty}\left(-\omega^2 m_{kn}^{\mu} + c_{kn}^{M\mu}\right)\mu_n = 0 \text{ for } k = 1....\infty \tag{20}$$

Here, the non-zero m_{ij}^{ξ} for $i, j < 4$ follow from (1)–(3) and are $m_{11}^{\xi} = m_{22}^{\xi} = m_T$, $m_{33}^{\xi} = I_{33}$ and $m_{13}^{\xi} = m_{31}^{\xi} = -z_G m_T$. The generalised mass coefficients m_{ij}^{ξ} for $i, j > 3$ associated with the normal deformation modes are given as $m_{ij}^{\xi} = m_M \int_{S_M} U_i U_{(j-3)} \mathrm{d}s$. The generalised mass coefficient m_{kn}^{μ} associated with the tangential deformation modes are given as $m_{kn}^{\mu} = m_M \int_{S_M} U_k U_n \mathrm{d}s$. Expressions for the structural stiffness coefficients $c_{ij}^{M\xi}$, $c_{kn}^{M\mu}$, $c_{in}^{M\xi\mu}$ and $c_{kj}^{M\mu\xi}$ are given in Appendix A. a_{ij} are the total generalised added mass coefficients with contributions from the internal and external added mass, b_{ij} are the generalised wave radiation damping coefficients from the external problem, c_{ij} are the generalised hydrostatic restoring coefficients. The non-zero coefficients for $i, j < 4$ are c_{22} and c_{33} (see (25) and (26)). The values of c_{ij} for $i, j > 3$ are given by (28). f_i^{exc} are the generalised wave excitation forces (see (40)). The evaluation of the restoring coefficients will now be described in the following section.

2.4. Restoring forces and moments

The restoring forces are both due to structural restoring and hydrostatic restoring, expressions for first the structural restoring and than the hydrostatic restoring will now be given.

2.4.1. Structural restoring forces and moments

The tension forces on the floaters from the membrane are illustrated in Fig. 3. The first order net tension total contribution from the dynamic tension forces in horizontal and vertical direction on the two floaters of the CFFC become

$$f_1^T = -T_0(\hat{\psi}(-\psi_e) + \hat{\psi}(\psi_e))\sin\psi_e - (\tau(\psi_e) - \tau(-\psi_e))\cos\psi_e \tag{21}$$

$$f_2^T = -(\tau(-\psi_e) + \tau(\psi_e))\sin\psi_e + T_0(\hat{\psi}(\psi_e) - \hat{\psi}(-\psi_e))\cos\psi_e \tag{22}$$

for small dynamic angles $\hat{\psi}$. Here the dynamic strain $\hat{e}$ and the dynamic angle $\hat{\psi}$ are given by (12) and (13). The roll moment about the centre of gravity of the CFFC due to the tension loads on the floaters become

$$f_3^T = \left(R^2(\tau(\psi_e) - \tau(-\psi_e)) + z_e^2 T_0(\hat{\psi}(-\psi_e) + \hat{\psi}(\psi_e))\right)\sin\psi_e \tag{23}$$

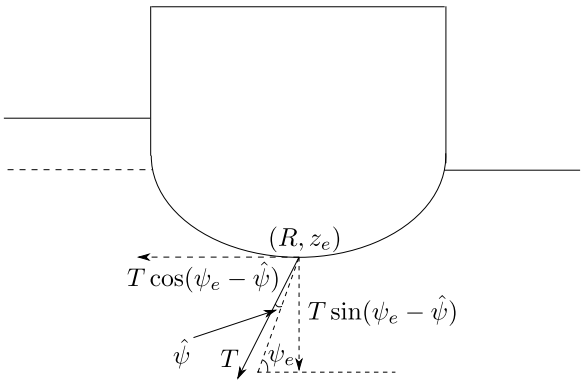

Fig. 3. Details at the right floater shown in Fig. 2 for the dynamic case, with dynamic angle $\hat{\psi}$ and tension $T = T_0 + \tau$. ψ_e is the attachment angle between the membrane and the right floater, z_e is the submergence of the floater and R is the radius of the membrane bag of the CFFC.

$$- \left(R^2 T_0 (\hat{\psi}(\psi_e) + \hat{\psi}(-\psi_e)) + z_e^2 (\tau(\psi_e) - \tau(-\psi_e)) \right) \cos\psi_e$$

Eqs. (21)–(23) using (12) and (13) can be written as restoring coefficients for $i < 4$ according to

$$f_i^T = -\sum_{j=4}^{\infty} c_{ij}^{M\xi} \xi_j - \sum_{n=1}^{\infty} c_{in}^{M\xi\mu} \mu_n. \tag{24}$$

2.4.2. Hydrostatic restoring forces and moments

If the hydrostatic pressure is integrated over the instantaneous position of the structure, it will contribute to restoring forces and moments. The change of hydrostatic pressure do not contribute to any restoring in sway. The only restoring in sway (ξ_1) would come from a mooring system. Since in this model the whole internal water moves as a rigid body when considering heave (ξ_2), there is no relative change in hydrostatic pressure internally. When we consider roll, there are contributions from the internal water as described in Faltinsen and Timokha (2009, page 79). The restoring coefficients in heave (c_{22}) and roll (c_{33}) by considering both internal and external contributions are given by

$$c_{22} = \rho_w g A_w(z_e), \tag{25}$$

$$c_{33} = -m_T g z_G + \rho_w g \left(\nabla z_B + \int_{A_w} y^2 dy - \overbrace{\frac{\rho_{wi}}{\rho_w} \left(\frac{1}{12} b_t^3 + \int_{Q_0^{(i)}} (\Delta h + z) dQ \right)}^{\text{Tank correction terms}} \right). \tag{26}$$

When defining some of the variables in (25) and (26), we refer to a fictitious rigid body including the floaters, the membrane and the water inside. Then, $A_w(z_e)$ is the waterplane area of the fictitious body, defined in 2D as $A_w(z_e) = 2(R + a(z_e))$. g is the gravitational acceleration. ∇ is the displaced volume of water of the fictitious body per unit length; z_G is the combined centre of gravity of the floaters and membrane of the CFFC. z_B is the $z-$ coordinate of the centre of buoyancy of the fictitious body and $b_t = 2(R - a(z_e))$ is the internal distance between the floaters at the free surface, and $a(z_e)$ is the submergence dependent width of the floater at the free surface. ρ_{wi} is the density of the water inside the cage, which can differ from the outside density, $Q_o^{(i)}$ is the internal water domain inside the CFFC and Δh is the difference in free surface levels between the inside domain and the surrounding water.

The generalised pressure loads due to a change in the hydrostatic pressure integrated over the instantaneous body surface will give a hydrostatic restoring force for the normal structural deformation modes. When considering change in the hydrostatic pressure due to the elastic deformation, we introduce first the change $U_{j-3}(\psi_0)\xi_j n_z$ that the normal deformation $U_{j-3}(\psi_0)\xi_j$ causes in vertical motion. Here n_z is the external surface normal vector component in the vertical direction when the body is at rest. Then we must account for a possible density difference $\Delta\rho = \rho_{wi} - \rho_w$ between the internal and external water. It means that the change in hydrostatic pressure loading on the membrane is

$$-\Delta\rho_w g U_{j-3}(\psi_0)\xi_j n_z. \tag{27}$$

The unit normal vector of the internal and external domain points in the opposite direction. We assume that the mean wetted external and internal membrane surface are approximately equal $S_M^{(i)} \approx S_M^{(e)}$, which is plausible as long as the thickness of the membrane d is small. The coupled restoring coefficients c_{kj} can be calculated by

$$\sum_{j=4}^{\infty} c_{kj}\xi_j = -\Delta\rho_w g \int_{S_M^{(e)}} \sum_{j=4}^{\infty} U_{(j-3)}(\psi_0) n_z U_{(k-3)}(\psi_0)\xi_j \mathrm{ds} \text{ for } j, k > 4. \tag{28}$$

This means that we will only have an additional restoring due to the normal structural deformation modes if the density of the internal and external liquid differ ($\Delta\rho \neq 0$). For limited density differences, the restoring coefficients of the structural deformation modes are small compared to the restoring coefficients of heave and roll.

Several papers have studied the effect of hydrostatic restoring loads for elastic bodies; (Malenica et al., 2015, 2009; Senjanovic et al., 2008; Newman, 1994). The given calculations deviate from these studies. Common for all of the cited papers are that they define the structural modes in a Cartesian *Oxyz* coordinate system. This complicates the calculations and leads to other terms. Senjanovic et al. (2008) and Newman (1994) only considered the restoring from the hydrostatic pressure on the external body, and did not account for hydrostatic pressure from any internal liquid. (Malenica et al., 2015, 2009) considers hydrostatic pressure in both an internal and an external domain, but have a different free surface condition for the internal domain, leading to a restoring term from the rise of the free surface, which is included in the internal added mass expressions.

The evaluation of the generalised hydrodynamic pressure loads will now be described in the following section.

2.5. Hydrodynamic pressure loads

The pressure loads are divided into external and internal pressure loads. We will start by looking at the external pressure loads.

2.5.1. Generalised hydrodynamic external pressure loads

To find the total dynamic pressure difference on the membrane we start by finding the external flow and resulting generalised pressure loads. We consider a 2D CFFC in incident regular waves of amplitude ζ_a, with wave number k and frequency ω at constant depth h in steady state oscillatory conditions. The wave steepness is small, and linear potential flow theory of incompressible water is assumed. It implies that flow separation is neglected and viscous flow is concentrated in thin body boundary layers not affecting the potential flow. For linear waves propagating in the y-direction, Faltinsen (1990) gives the velocity potential for incident waves at finite constant depth h as:

$$\phi_0 = \frac{g\zeta_a}{\omega}\frac{\cosh k(z+h)}{\cosh kh}e^{(\mathrm{i}\omega t - \mathrm{i}ky)}, \tag{29}$$

with the dispersion relation $\frac{\omega^2}{g} = k\tanh kh$.

The presence of the body modifies the flow field in terms of a linear diffraction velocity potential ϕ_d and radiation velocity potentials $\phi_j^{(e)}$ associated with the body motions. The total external velocity potential Φ_e is given as:

$$\Phi_e = \phi_0 + \phi_d + \sum_{j=1}^{\infty}\phi_j^{(e)}\xi_j. \tag{30}$$

Here $j = 1, 2, 3$ represent the rigid body motions in sway, heave and roll, and $j = 4..\infty$ represent the normal deformation modes of the membrane. The tangential deformation modes cannot cause flow within linear potential flow theory.

The boundary value problem satisfies:

$$\frac{\partial^2\Phi_e}{\partial y^2} + \frac{\partial^2\Phi_e}{\partial z^2} = 0 \text{ in } Q_0^{(e)}, \tag{31}$$

$$\frac{\partial\Phi_e}{\partial z} = 0 \text{ at } z = -h, \tag{32}$$

$$-\omega^2\Phi_e + g\frac{\partial\Phi_e}{\partial z} = 0 \text{ on } z = 0, \tag{33}$$

in addition to body boundary conditions and a radiation condition ensuring outgoing far-field waves caused by the body. Here $Q_0^{(e)}$ is the mean external liquid domain. The body boundary condition for the diffraction potential is:

$$\frac{\partial\phi_d}{\partial n} = -\frac{\partial\phi_0}{\partial n} \text{ on } S_M^{(e)} + S_{Fl}^{(e)}, \tag{34}$$

where $S_M^{(e)}$ and $S_{Fl}^{(e)}$ are the mean wetted external membrane surface and floater surface, respectively. $\frac{\partial}{\partial n}$ denotes the normal derivative to the mean wetted external body surface. The corresponding normal vector $\vec{n}$ has positive direction into the external water. Its components along the $y-$ and $z-$ axes are denoted n_y and n_z, respectively. The body boundary conditions for the radiation problems are:

$$\frac{\partial\phi_j^{(e)}}{\partial n} = \mathrm{i}\omega n_j^{(e)} \text{ on } S_M^{(e)} + S_{Fl}^{(e)}. \tag{35}$$

Here $j = 1, 2, 3$ represent the rigid body motions in sway, heave and roll. It follows that

$$n_j^{(e)} = \begin{cases} n_y & \text{for } j = 1 \\ n_z & \text{for } j = 2 \\ yn_z - zn_y & \text{for } j = 3. \end{cases} \tag{36}$$

Furthermore, $j = 4.\infty$ are the prescribed normal deformation motions. It implies for $j \geq 4$ that

$$n_j^{(e)} = \begin{cases} U_{j-3}(\psi_0) & \text{on } S_M^{(e)} \\ 0 & \text{on } S_{Fl}^{(e)}. \end{cases} \tag{37}$$

The far-field velocity potentials representing outgoing waves can be expressed as

$$\phi_R^{\pm} = \frac{g}{\omega} A^{(\pm)} \frac{\cosh k(z+h)}{\cosh kh} e^{(\mathrm{i}\omega t \mp \mathrm{i}ky)} \text{ for } y \to \pm\infty, \tag{38}$$

Here $A^{(+)}$ and $A^{(-)}$ represent far-field complex wave amplitudes and are unknowns in solving the problem.

Generalised added mass and damping terms for the external flow problem follows from properly integrating the time derivative of $\phi_j^{(e)}$, originating from the linear dynamic pressure part $-\rho_w \partial \Phi_e / \partial t$ in Bernoulli's equation. The expressions are given by

$$\mathrm{i}\omega\rho_w \int_{S_{Fl}^{(e)}+S_M^{(e)}} \phi_j^{(e)} n_k^{(e)} \xi_j \mathrm{d}s = \left(\omega^2 a_{jk}^{(e)}(\omega) - \mathrm{i}\omega b_{jk}^{(e)}(\omega)\right)\xi_j \tag{39}$$

where $a_{kj}^{(e)}$ and $b_{kj}^{(e)}$ are the external 2D added mass and damping contribution in k direction, due to a motion in j direction.

The generalised excitation loads f_k^{exc} are

$$\mathrm{i}\omega\rho_w \int_{S_{Fl}^{(e)}+S_M^{(e)}} (\phi_0 + \phi_d) n_k^{(e)} \mathrm{d}s = f_k^{exc}(\omega) \tag{40}$$

Relations between the damping and the far-field wave amplitude, and between excitation force and damping, together with a symmetry relation based on Green's second identity were used to verify the correctness of the numerical code. A relation between the damping coefficient $b_{jj}^{(e)}$ and the far field wave amplitude can be derived based on conservation of energy. The expression is

$$b_{jj}^{(e)} = \frac{\rho_w g^2}{\omega^3} \left(\frac{|A_j^+|}{|\xi_j|}\right)^2 2kI_1. \tag{41}$$

where $I_1 = \int_{-h}^{0} \frac{\cosh^2 k(z+h)}{\cosh^2 kh} \mathrm{d}z = \frac{\sinh(kh)\cosh(kh)+kh}{2k\cosh^2 kh}$, which is consistent with Faltinsen and Timokha (2009) for rigid body motions.

For an infinitely long cylinder in beam sea, at infinite depth the excitation force amplitude $|f_{ja}^{exc}|$ has a known relation to the two-dimensional diagonal damping coefficient $b_{jj}^{(e)}$ for rigid body motion (Newman, 1962). For finite water depth and generalised to include normal membrane deformation modes this relation were found to be:

$$|f_{ja}^{exc}| = \zeta_a \sqrt{\frac{\rho_w g^2}{\omega} b_{jj}^{(e)} 2kI_1}. \tag{42}$$

Green's second identity tells that

$$\int_{\Sigma_{0e}+S_{Fl}^{(e)}+S_M^{(e)}+S_\infty} \left[\phi_j^{(e)} \frac{\partial \phi_k^{(e)}}{\partial n} - \phi_k^{(e)} \frac{\partial \phi_j^{(e)}}{\partial n}\right] ds = 0. \tag{43}$$

Here S_∞ are vertical control surfaces between $z = 0$ and $z = -h$ at $y = \pm\infty$. If we use (43) together with boundary conditions on the mean the free surface Σ_{0e}, S_∞ and on the mean wetted tank surface $S_{Fl}^{(e)} + S_M^{(e)}$, we can derive symmetry properties of the added mass and damping coefficients. For $S_{Fl}^{(e)} = 0$, indicating that there are either no floaters or the floaters are not submerged $a_{jk}^{(e)} = a_{kj}^{(e)}$ and $b_{jk}^{(e)} = b_{kj}^{(e)}$ for all j, k. However, when $S_{Fl}^{(e)}$ is non-zero the relations will only hold for $j, k < 4$ and $j, k \geq 4$. If should be commented that $S_{Fl}^{(e)} = 0$ is not a realistic scenario as the cage must have partly submerged floaters to be stable in roll.

2.5.2. Internal water pressure loads

Linear potential flow theory of an incompressible liquid is assumed for the internal domain. For the internal flow it is most convenient to operate in a tank fixed reference system. The coordinate axes of the tank fixed coordinate system at tank rest are parallel to the axes of the global body fixed coordinate system. Translatory motions are defined along tank fixed axes and related to the origin of the internal tank fixed coordinate system. At rest, the origin of the tank fixed reference system is placed at the origin of the global inertial coordinate system, see Fig. 4. Since we assume small motions

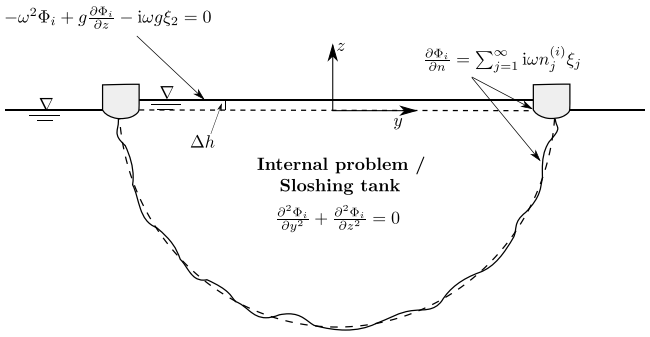

Fig. 4. Boundary conditions for a two-dimensional half circular closed flexible fish cage with floaters in the frequency domain.

and deformations, origins of the inertial reference system and tank − fixed reference system at rest are collocated. Due to the assumptions of small motions and deformations the difference the representation of the rigid body motions and membrane deformations are the same when considering the internal and external problems. In the tank fixed coordinate system, Bernoulli's equation in its original form must be modified to an accelerated coordinate system (Faltinsen and Timokha, 2009, page 47). As long as we operate with a linear system the linearised version of the pressure, or more precisely excess pressure relative to atmospheric pressure will be

$$p = -\rho_{wi}\frac{\partial \Phi_i}{\partial t} - \rho_{wi} g \eta_4 y - \rho_{wi} g(z - \Delta h), \tag{44}$$

with Φ_i as the internal velocity potential. The equation is consistent with that the excess pressure is zero at $z = \Delta h$ when the tank is at rest.

The internal velocity potential Φ_i can be expressed as

$$\Phi_i = \sum_{j=1}^{\infty} \phi_j^{(i)} \xi_j. \tag{45}$$

The velocity potential $\phi_j^{(i)}$ satisfies

$$\frac{\partial^2 \phi_j^{(i)}}{\partial y^2} + \frac{\partial^2 \phi_j^{(i)}}{\partial z^2} = 0 \text{ in } Q_0^{(i)}, \tag{46}$$

$$\frac{\partial \phi_j^{(i)}}{\partial n} = \mathrm{i}\omega n_j^{(i)} \text{ on } S_M^{(i)} + S_{Fl}^{(i)}. \tag{47}$$

Here $Q_0^{(i)}$ is the mean internal liquid domain, $S_{Fl}^{(i)}$ is the mean internal wetted floater surface and $S_M^{(i)}$ is the internal wetted surface of the membrane.

The internal normal vector $\vec{n}^{(i)} = (n_y^{(i)}, n_z^{(i)})$ has positive direction into the internal water. We define similarly as for the external problem

$$n_j^{(i)} = \begin{cases} n_y^{(i)} & \text{for } j = 1 \\ n_z^{(i)} & \text{for } j = 2 \\ y n_z^{(i)} - z n_y^{(i)} & \text{for } j = 3, \end{cases} \tag{48}$$

and introduce for the prescribed normal deformation modes for $j = 4$. that

$$n_j^{(i)} = \begin{cases} -U_{j-3}(\psi_0) & \text{on } S_M^{(i)} \\ 0 & \text{on } S_{Fl}^{(i)}. \end{cases} \tag{49}$$

At the free surface, we linearise (44) at the internal free surface $z - \Delta h - \zeta_i = 0$, where ζ^i describes the internal wave elevation relative to the movable, tank fixed coordinate system. We then arrive at the linearised dynamic free surface conditions in the body fixed coordinate system:

$$\frac{\partial \Phi_i}{\partial t}|_{\Sigma_0^{(i)}} + y g \eta_4 + g\zeta^i = 0. \tag{50}$$

Here, $\Sigma_0^{(i)}$ is the mean free surface inside the tank. The kinematic linearised free surface conditions is (Faltinsen and Timokha, 2009, page 198):

$$\frac{\partial \Phi_i}{\partial z} - \dot{\xi}_2 - y\dot{\xi}_3 - \frac{\partial \zeta^i}{\partial t} = 0 \tag{51}$$

In addition, conservation of liquid mass

$$\int_{\Sigma_0^{(i)}} \zeta^i dy = \int_{S_M^{(i)}} \sum_{j\geq 4} n_j^{(i)} \xi_j \mathrm{d}s, \tag{52}$$

must be satisfied. Eq. (51) is not the same as in an Earth-fixed coordinate system. Changes had to be made to include the inertial terms due to the rigid body motions and due to the effect of the gravitational acceleration in the body fixed coordinate system. Eq. (52) expresses that the free surface elevation must be consistent with conservation of liquid volume. If $\int_{S_M^{(i)}} n_j^{(i)} \xi_j \mathrm{d}s \neq 0$ for $j \geq 4$ for a given non-zero ξ_j, a constant change in the free surface exist, meaning that the free surface will not be located at $z = \Delta h$. By combining (51) with the time derivative of (50) in the frequency domain, we get the linearised free surface condition

$$-\omega^2 \Phi_i + g\frac{\partial \Phi_i}{\partial z} - \mathrm{i}\omega g \xi_2 = 0. \tag{53}$$

As a consequence of properly integrating the time derivative part of the pressure as given by Bernoulli's equation related to the tank fixed coordinate system, we obtain the following added mass coefficients $a_{jk}^{(i)}$

$$\mathrm{i}\rho_{wi}\omega \int_{S_{Fl}^{(i)}+S_M^{(i)}} \phi_j^{(i)} n_k \xi_j \mathrm{d}s = \omega^2 a_{jk}^{(i)}(\omega)\xi_j \tag{54}$$

where ρ_{wi} is the density of the water inside the CFFC and $a_{jk}^{(i)}$ is the internal 2D added mass contribution in j direction, due to a motion in k direction. There are no damping coefficients according to potential flow theory for the interior problem. The hydrodynamic damping coefficients associated with viscous boundary layer at the wetted body surface will be neglected. However, this damping is in reality small (Faltinsen and Timokha, 2009, page 377).

Symmetry of coefficients can also be used to verify the internal added mass coefficients, by using Green's second identity as was done for the external problem. Due to the free surface condition for heave, we will not have that $a_{jk}^{(i)} = a_{kj}^{(i)}$ for coupling terms between heave and the normal deformation modes. When $S_{Fl}^{(i)} > 0$, the relation will only hold for all j, k except $j, k = 3$.

The internal relative wave elevation ζ^i follows from the dynamic free-surface condition (50):

$$\zeta^i = -\frac{i\omega}{g} \sum_{j=1}^{\infty} \phi_j^{(i)} \xi_j|_{\Sigma_0^{(i)}} - y\eta_4. \tag{55}$$

2.5.3. Numerical flow method

To find the hydrodynamic pressure loads on the CFFC, a numerical solution using the Harmonic Polynomial Cell (HPC) method has been implemented. The HPC method is a field method initially described by Shao and Faltinsen (2014a,b) to solve the Laplace equation with boundary conditions for an unknown velocity potential together with initial conditions in the time domain and periodicity condition in the frequency domain. In the HPC method, the local expression of the velocity potential within a cell uses harmonic polynomials. Hence, the governing equation is satisfied naturally. The connectivity between different cells is built by overlapping the local expressions. A key feature of the HPC method is in using higher-order local expressions satisfying Laplace equation, which means that we can expect a better accuracy than for many other low order field and boundary integral formulations presently used. Moreover, the HPC method operates with a sparse coefficient matrix, so that many existing numerical matrix solvers can solve the associated problem efficiently. See Appendix C for the used equations.

For the rectangular tank with a flexible wall analysed in Strand and Faltinsen (2017) the computational domain was rectangular, and easily discretised with quadratic cells. Since the geometry of the CFFC is not rectangular, a method to account for a non-rectangular boundary must be used. Ma et al. (2017) have found that the HPC method have best accuracy for quadratic grid cells, and that severe stretching or distortion of the cells should be avoided. Inspired by Hanssen et al. (2015), who successfully implemented an immersed boundary method (IBM) for a moving body we use a fixed Cartesian quadratic grid, with an immersed boundary method to capture the boundary. An alternative to using an immersed boundary method for the HPC is to use a boundary fitted multigrid approach as done in Hanssen et al. (2017), this could be highly relevant for a non-linear scheme but is not pursued further for this linear model.

Ghost nodes inside (for the external problem) and outside (for the internal problem) the body are applied to reconstruct the velocity at the immersed boundary (Hanssen et al., 2015). The body-boundary condition on immersed boundaries are projected onto the surrounding ghost nodes. The applied code uses one layer of ghost nodes and uses the harmonic polynomials of the HPC method to interpolate the coordinate of the boundary to the ghost cell. The ghost nodes are connected to cells inside the liquid domain.

Table 1
Case dimensions for a 2D CFFC with floaters. R is the radius of the semi-circular bag, d is the thickness of the fabric, E is the elasticity module of the fabric, ρ_N is the density of the fabric, ρ_w is the applied density of salt water, R_F is the radius of the floater, z_e is the floater submergence, T_0 is the static tension in the membrane, ψ_e is the top angle at the right floater and m_{Fl} is the mass of the floater per meter.

R	d	E	ρ_N	$\Delta h/R$	R_F	z_e/R_F	$T_0/\rho_w g R^2$	ψ_e	m_{Fl}
12.5 m	$7.5 \cdot 10^{-4}$ m	$2.25 \cdot 10^9$ Pa	1150 kg/m^3	$15.0 \cdot 10^{-3}$	1.25	−0.92	$15.0 \cdot 10^{-3}$	$\frac{\pi}{2}$	10.4 kg/m

The numerical HPC framework was implemented in Python. To find the immersed boundary, the Python package "Shapely" was used. Based on predefined structural input points defining the geometry, a point on the boundary inside the cell based on linear approximation between the predefined structural input points was found.

2.5.4. Numerical theory for the external domain

The far-field velocity potential assumes that the domain has infinite horizontal extent. However, according to Billingham and King (2009), the far-field velocity potential is a good approximation as long as $l \geq 4h$, where l is the total length of the domain.

The velocity potentials caused by the body have symmetric and antisymmetric properties with respect to a symmetry line containing the z-axis. The later fact follows from symmetry and antisymmetry properties of the generalised normal components of the mean submerged body surface $n_j^{(e)}$. $n_1^{(e)}$ and $n_3^{(e)}$ are antisymmetric while $n_2^{(e)}$ is symmetric. When $j > 3$, the odd membrane modes ($(j-3) = 1, 3, 5...$) are symmetric while the even membrane modes ($(j-3) = 2, 4, 6...$) are antisymmetric. Furthermore, the body boundary condition for the diffraction potential can be divided into symmetric and antisymmetric parts. The symmetric and antisymmetric properties allow us to only consider half the water domain. When the body boundary condition is antisymmetric, the far-field complex wave amplitude $A_j^{(+)} = -A_j^{(-)}$ and $\phi_j^{(e)} = 0$ at the symmetry line. The properties for symmetric potentials are $A_j^{(+)} = A_j^{(-)}$, and $\partial\phi_j^{(e)}/\partial y = 0$ at the symmetry line. These conditions are used as a boundary conditions at the symmetry line. Due to the symmetry and antisymmetry properties of the system it is sufficient to only consider the right part of the tank. The boundary condition on the right wall of the tank then becomes

$$\frac{\partial \phi_j^{(e)}}{\partial y} = -\mathrm{i}\omega A_j^{(+)} \frac{\cosh k(z+h)}{\sinh kh} e^{(\mathrm{i}\omega t - \mathrm{i}k\frac{l}{2})} \text{ on } y = \frac{l}{2}. \tag{56}$$

3. Case study of a CFFC in waves

To build knowledge of the 2D response of the closed flexible fish cage in waves a case study based on the given system description have been done. The wave-induced response of a CFFC with a semi-circular static membrane equilibrium geometry, with overfilling and no density differences has been analysed in the frequency domain, at finite water depth for depth-to-radius ratio $h/R = 4.0$. The density of sea water is $\rho_w = 1025$ kg/m^3. The non-dimensional squared frequency range $0.2 \leq \omega^2 R/g \leq 5.6$ is considered, which includes wave peak periods in the weather range from moderate to extreme in NS9415 (Norwegian standard) for a CFFC with full scale radius $R = 12.5$ m. Furthermore, the three lowest natural sloshing frequencies occur in the considered frequency domain. A half circular shape is a good approximation of the shape as long as the mass forces of the membrane in water are much lower than the overpressure forces, meaning that $\pi R d g(\rho_N - \rho_w) \ll g b_t \Delta h \rho_w$. Here $g b_t \Delta h \rho_w = 44777.3 \gg \pi R d g(\rho_N - \rho_w) = 36.1$, which satisfies the requirement. The geometry of the 2D membrane is assumed semi-circular, the top angle $\psi_e = \pi/2$ and $S_M = \pi R$, which simplifies the expressions for the structural deformations found in Section 2.2. The system equations for a semi-circular membrane are given in B. The moment of inertia in roll I_{33} is calculated as $I_{33} = (0.53\pi\rho_c dR + 2m_{Fl})R^2$ and the centre of gravity z_G of the combined membrane and floaters are set equal to zero. Relevant used full scale values are given in Table 1. Compared to the floaters used today, the floaters used here are large floaters. A finite number of modes ξ_i, $i = 1...I$ and μ_k, $k = 1..K$ are considered, where I and K follow from convergence studies, see Strand and Faltinsen (2017) for more information.

A structural damping of both the normal and tangential membrane modes have been added to the structural model of the membrane. The material that most resembles the membrane used in CFFCs, that have available figures on the structural damping is nylon. The damping level of nylon is dependent on humidity, frequency and temperature (Quistwater and Dunell, 1958). Based on the frequency range and the humidity (wet) a structural damping of 2% of the critical damping was chosen for each mode. Coupled structural damping effects were neglected. Instead of using a damping related to the critical damping, a Rayleigh damping model with mass and structural stiffness terms is possible. Both these damping models were tried and the critical damping model appeared to have the best convergence related to the number of tangential membrane modes. The critical damping of motion j for $j > 3$ for the normal membrane modes have been calculated as $b_j^{str,\xi} = d_c(m_{ij}^{\xi} + a_{jj})\sqrt{\frac{c_{M\xi,ij}+c_{ij}}{m_{jj}^{\xi}+a_{jj}}}$ where d_c is the damping ratio. For the tangential membrane modes the critical damping of mode n have been calculated as $b_j^{str,\mu} = d_c m_{jj}^{\mu}\sqrt{\frac{c_{kn}^{M\mu}}{m_{jj}^{\mu}}}$. For the future the structural damping of the actual used fabric, for a wet condition, for the relevant temperatures and frequency range should be found.

We will in this chapter start with describing the results of the added mass and damping coefficients of the CFFC. Then the response of a rigid CFFC will be analysed to have results for a structure that the results for a fully flexible CFFC can be compared against. Then the rigid body motion response of the CFFC and the flexible deformations of the modes will be analysed. The internal wave amplitude inside the CFFC will so be considered. Before the dynamic tension in the system is considered with the aim to see if the requirements of the given linear theory is met related to tension. At the end we will look at the rigid body motion response of a CFFC with model parameters used in model scale experiments of a CFFC.

3.1. Added mass and damping coefficients

External non-dimensional added mass, damping and excitation, and non-dimensional internal added mass have been found using the HPC method.

For a hemicircle (CFFC without floaters) reference values for the pressure loads can be found both related to the external added mass and damping for sway and heave, and for the sloshing eigenfrequencies for the given frequency range. Results for a hemicircle are in good agreement related to added mass and damping in heave and sway (Faltinsen and Timokha, 2009; Bai and Yeung, 1974), and sloshing eigenfrequencies (Faltinsen and Timokha, 2009). The relation between the far-field wave amplitude $|A_j^+|$ and the estimated external diagonal damping coefficient given by (41), together with the relation between the calculated two-dimensional diagonal damping coefficient $b_{jj}^{(e)}$ and the excitation force for finite depth given by (42) have been used for verification of the code. In addition, the L_2 error between the calculated and estimated damping, and between the calculated and estimated excitation force have been used as a measure of convergence. Green's second identity for the external and internal problem by (43) have been used to verify convergence through symmetry of coefficients.

3.1.1. External added mass and damping CFFC

An external computational domain with water depth to bag radius ratio $h/R = 4$ and horizontal extent-to-water depth ratio $l/h = 4$, where only the right half of the tank (on the right side of the symmetry line) were used. The external added mass and damping coefficients in sway, heave and roll for a CFFC in waves are comparable in size and behaviour to the coefficients for a hemicircle. However, opposite to the hemicircle, the structure have a small non-zero added mass, damping and excitation in roll due to the presence of the floaters.

The added mass and damping coefficients of the first two structural modes are comparable in magnitude to the coefficients in sway and heave. The magnitude of the added mass and damping decreases with increasing mode number. This can also be seen analytically by considering the high frequency asymptotic behaviour of symmetric modes and is related to both the oscillatory behaviour of the pressure and the multiplying mode. For generalised mode numbers $j > 10$ it appears that the added mass becomes frequency independent.

3.1.2. Internal added mass CFFC

The internal added mass coefficients of the CFFC have been analysed. Within the given non-dimensional frequency range three sloshing eigenfrequencies exist; k_1R, k_2R and k_3R. The absolute value of the sway added mass becomes infinite at the sloshing eigenfrequencies k_1R and k_3R, with both negative and positive values for the sway added mass, with a large frequency dependence at k_1R and k_3R. Compared to a hemicircle, when floaters are added to the geometry and the equilibrium geometry is used for the analysis, the results will deviate from reference values for the sloshing frequencies for a hemicircle given by Faltinsen and Timokha (2009). All the new non-dimensional eigenfrequencies k_1R, k_2R and k_3R, are larger than the reference values from Faltinsen and Timokha (2009) k_1^*R, k_2^*R and k_3^*R, which is consistent with the comparison theorem described by Faltinsen and Timokha (2009, page 150). The added mass in heave is constant and equal to the mass of the enclosed water.

The even membrane deformation modes have a sloshing resonance at the second sloshing eigenfrequency, while the odd membrane deformation modes have sloshing resonances at the first and third sloshing frequencies. The internal added mass coefficients of the even membrane deformation modes do not approach a constant value when ω goes to zero. This is because the internal added mass coefficient for these modes include a restoring coefficient associated with the quasi-static hydrostatic pressure change due to the change in mean free surface, as described in Strand and Faltinsen (2017). The internal added mass coefficient can then be described according to $a_{jk}^{(i)}(\omega) = \frac{c_{jk}^{(i)}}{\omega^2} + a_{jk}^{(i*)}(\omega)$. Where $c_{jk}^{(i)}$can be calculated as $c_{jk}^{(i)} = \frac{\rho_w g R}{b_t} \int_{\pi/2}^{-\pi/2} (\int_{-\pi/2}^{\pi/2} U(\psi_0)_{k-3} \mathrm{d}\psi) U(\psi_0)_{j-3} \mathrm{d}\psi$ for $j, k > 3$. Heave will also have a coupling restoring coefficient due to this effect which is $c_{2k}^{(i)} = \frac{\rho_w g R}{b_t} \int_{-\pi/2}^{\pi/2} U(\psi_0)_{k-3} \mathrm{d}\psi$ for $k > 3$.

3.2. Wave-induced motion of a rigid CFFC

For verification purposes and as a base case the response of a rigid CFFC is first considered. This means that the membrane is considered totally rigid with zero deformations. The linear steady-state motion can be expressed as

$$\xi_j = \xi_{ja} \cos(\omega t + \epsilon_j), \tag{57}$$

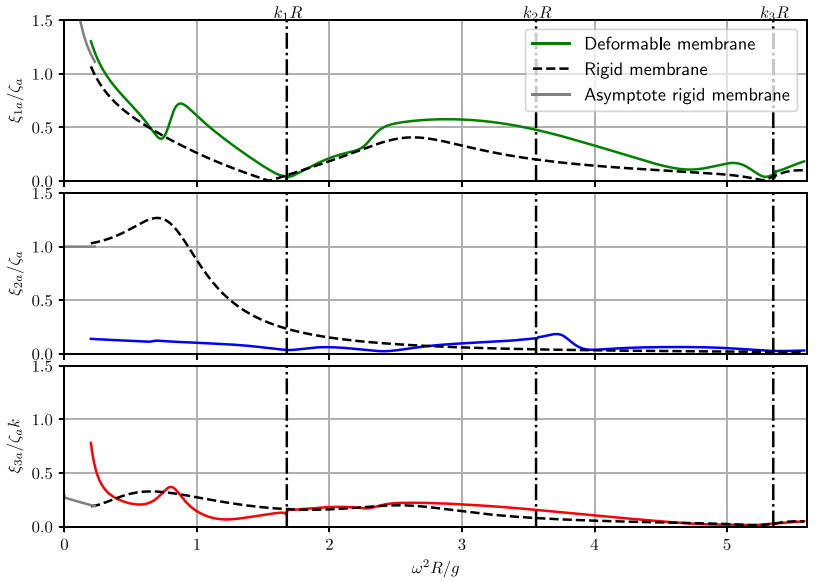

Fig. 5. Transfer functions of motion of CFFC for sway (top), heave (middle) and roll (bottom), with and without the effect of the deformable membrane versus non-dimensional squared frequency $\omega^2 R/g$. k_1R, k_2R and k_3R are non-dimensional natural sloshing frequencies for the CFFC.

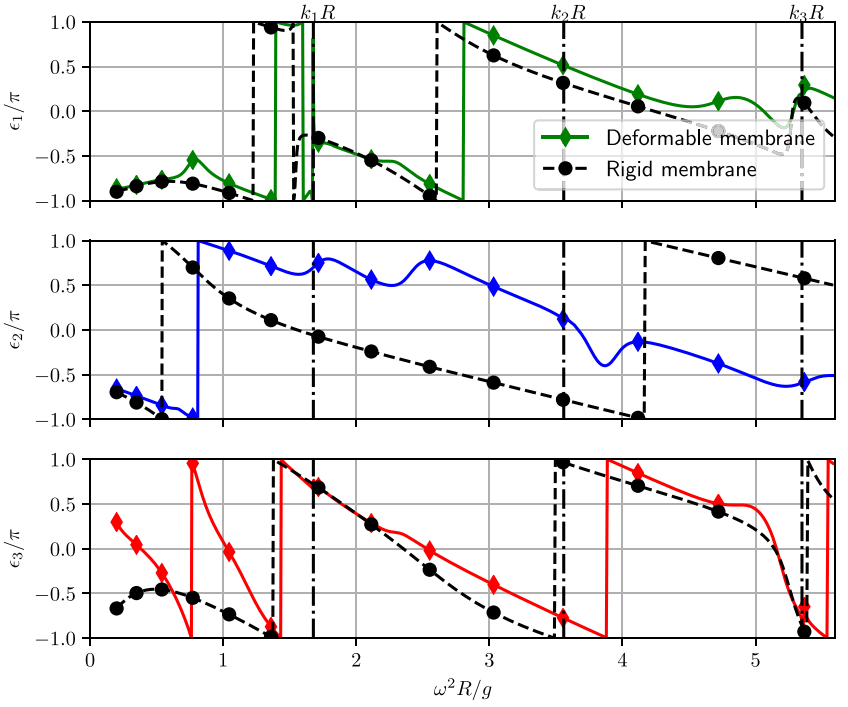

Fig. 6. Phase of motion of CFFC for sway (top), heave (middle) and roll (bottom), with and without the effect of the membrane versus non-dimensional squared frequency $\omega^2 R/g$. k_1R, k_2R and k_3R are non-dimensional sloshing frequencies for the CFFC.

where the phase angle ϵ_j can be related to the incident wave elevation $\zeta = \zeta_a \sin(\omega t - ky)$. The transfer functions ξ_{ja}/ζ_a for the coupled body motions in sway, heave and roll of the rigid CFFC as well as the CFFC with the deformable membrane are plotted in Fig. 5. The phases in sway, heave and roll of the coupled rigid body motions of the rigid CFFC as well as the CFFC with the deformable membrane are plotted in Fig. 6.

To examine the correctness of the results, we investigate the behaviour of the rigid body motions when the frequency approaches zero ($\omega \to 0$). We introduce $\omega\sqrt{R/g}$ as a small parameter in addition to ζ/R being small. We denote z_m as

an average vertical coordinate of the structure, for instance can z_m be z_B. Taylor expansion of the linear dynamic incident pressure p_0 about $(y,z)=(0,z_m)$ gives

$$p_0=\rho_w g\zeta_a\left(\frac{\cosh k(z_m+h)}{\cosh kh}\sin(\omega t)+zk\frac{\sinh k(z_m+h)}{\cosh kh}\sin(\omega t)-yk\frac{\cosh k(z_m+h)}{\cosh kh}\cos(\omega t)\right)+O(\frac{\omega^2R}{g}) \tag{58}$$

It follows by using Gauss theorem that the linear Froude–Kriloff roll moment about $(y,z)=(0,z_m)$ correct to $O(\frac{\omega^2R}{g})$ is equal to

$$f_3^{FK}=-\rho_w gk\zeta_a\frac{\cosh k(z_m+h)}{\cosh kh}\int_{S_M^{(e)}+S_{fl}^{(e)}}y(zn_y-yn_z)ds\cos(\omega t)=-\rho_w gk\zeta_a\left(\int_{A_w}y^2\mathrm{d}y+z_B\nabla\right)\frac{\cosh k(z_m+h)}{\cosh kh}\cos(\omega t). \tag{59}$$

Here, ∇ is the displaced volume of the fictitious body, consisting of the floaters, the membrane and the water inside the CFFC. The diffraction potential ϕ_d satisfies correctly to $O(\frac{\omega^2R}{g})$ the body boundary condition

$$\frac{\partial\phi_d}{\partial n}=-n_y\frac{\partial\phi_0}{\partial y}|_{(y=0,z=z_m)}-n_z\frac{\partial\phi_0}{\partial z}|_{(y=0,z=z_m)}$$

It is the antisymmetric part of ϕ_d that gives a roll moment. The problem is according to the body boundary condition similar to study forced sway with velocity $-\frac{\partial\phi_0}{\partial y}$ at $(y,z)=(0,z_m)$. It follows then that the diffraction potential gives the roll moment

$$a_{31}^{(e)}kg\zeta_a\frac{\cosh k(z_m+h)}{\cosh kh}\cos(\omega t).$$

We can similarly evaluate the wave excitation forces in sway and heave. The lowest order terms in the equations of motions become

$$-\omega^2(m_T+a_{11})\xi_1=(\rho_w\nabla+a_{11}^{(e)})\frac{\cosh k(z_m+h)}{\sinh kh}\cos(\omega t). \tag{60}$$

$$c_{22}\xi_2=\rho_w g\zeta_a\frac{\cosh k(z_m+h)}{\cosh kh}\sin(\omega t). \tag{61}$$

$$c_{33}\xi_3-\omega^2(a_{31}-z_Gm_T)\xi_1=gk\zeta_a\left(-\rho_w\left[\int_{A_w}y^2\mathrm{d}y+z_B\nabla\right]+a_{31}^{(e)}\right)\frac{\cosh k(z_m+h)}{\cosh kh}\cos(\omega t). \tag{62}$$

Here, m_T is the combined mass of the membrane and floaters. All the added masses a_{jk} are frequency dependent and are supposed to be evaluated at $\omega\to 0$. However, we use the calculated values at the lowest numerically considered frequency $\omega^2R/g=0.2$ which differ from the values at $\omega=0$.

For the sway motion, the asymptote of the sway motion approaches $\frac{\xi_{1a}}{\zeta_a}\to\frac{\cosh k(z_m+h)}{\sinh kh}\to\frac{1}{\tanh kh}$ when $\omega\to 0$. Physically this means that the horizontal CFFC motion approaches the horizontal incident wave particle motion. The latter asymptotic behaviour is consistent with the numerical results in Fig. 5. For the sway phase asymptote, the sway motion should approach the horizontal incident wave particle motion. Then it is required that $\epsilon_1\to\pm\pi$. It can be observed from Fig. 6 that this is satisfied.

The asymptote for heave is according to Eq. (61) $\xi_{2a}/\zeta_a\to 1$ when $\omega\to 0$, which also is consistent with the results plotted in Fig. 5. Physically this implies that the vertical motion of the CFFC follows the vertical incident wave particle motion. The heave phase is consistent with that the CFFC follows the vertical incident wave particle motion i.e $\epsilon_2\to-\pi/2$.

When it comes to roll, the prediction based on Eq. (62) seem to over predict the behaviour. A reason to that is that the wave excitation moment is overpredicted due to too large diffraction moment. The exact calculation of the moment show small influence of the diffraction moment. The later have independently been confirmed by using the Newman relation, see Eq. (42). The Froude–Kriloff moment according to Eq. (59) agrees well with the exact calculations. Using only the Froude–Kriloff moment as the excitation moment in the asymptotic formulas gives good agreement with the direct calculation. Since $\frac{\xi_{1a}}{\zeta_a}\to\frac{\cosh k(z_m+h)}{\sinh kh}$ when $\omega\to 0$ and $z_G\approx 0$, Eq. (62) accounting only for the Froude–Kriloff moment as the excitation force can be rearranged to

$$\frac{\xi_{3a}}{\zeta_a k}=\frac{1}{c_{33}}\frac{\cosh k(z_m+h)}{\cosh kh}g\left(-\rho_w\zeta_a\left[\int_{A_w}y^2\mathrm{d}y+z_B\nabla\right]+a_{31}\right). \tag{63}$$

The asymptote of the coupled roll motion can be calculated based on (63) using $a_{31}(\omega_{min})$ as an estimate for $a_{31}(\omega=0)$, since $a_{31}(\omega=0)$ is not known. The estimate of the asymptote based on Eq. (63) is plotted in Fig. 5 and agrees well with the simulated results. A so low asymptote for the roll motion when the frequency approaches zero is a surprising result; for rigid free surface piercing bodies with no internal tanks the asymptote of the roll motion for very long waves usually follows the wave curvature, meaning that $\frac{\xi_{3a}}{\zeta_a k}\to 1$. However, liquid in internal tanks will in general have a destabilising effect on the roll motion. The first term in the tank correction terms in the expression for c_{33} in (26) is stabilising, while the second term is destabilising. Structures with internal tanks will therefore not follow the wave slope as expected for

rigid free surface piercing bodies (Faltinsen and Timokha, 2009, p 82). The explanation for the low asymptote in the given results is a combination of causes. First; the restoring term c_{33} is larger than the Froude–Kriloff force f_3, and the resulting asymptote is therefore below one. In addition has the coupling to sway a significant influence on the motion. For the phase of the roll motion to follow the phase of the wave slope, the roll phase ϵ_3 should approach $\pm\pi$. Based on Fig. 6, it could appear that the phase of the roll rigid motion approaches $-\pi$.

The behaviour of the rigid body motions around the sloshing eigenfrequencies should also be examined for consistency. Uncoupled sway and roll are zero at the first and third sloshing frequency. This is consistent with previous results as published by Newman (2005) and discussed in Faltinsen and Timokha (2009). For the CFFC in coupled sway and roll, the response is finite at the first and third sloshing frequency, as can be seen in Fig. 5. This is due to the coupling terms between sway and roll, which causes finite response at the natural sloshing frequency (Faltinsen and Timokha, 2009, page 102). Since the internal heave added mass is constant, the rigid body motion in heave is unaffected by sloshing.

The eigenfrequencies of the rigid body motions are now considered. Mooring is not accounted for in this problem, the sway motion will therefore not have any eigenfrequency. Heave has a damped eigenfrequency at the non-dimensional eigenfrequency $\frac{\omega_{n2}^2 R}{g} = 0.73$. The undamped eigenfrequency can be estimated as $\frac{\omega_{n2}^2 R}{g} = \frac{c_{22}R}{g(a_{22}+m_T)} = 0.79$. Since both sides of this expression are dependent on the frequency, the eigenfrequency have been found by finding the minimum of $|\frac{\omega_{n2}^2 R}{g} - \frac{c_{22}R}{g(a_{22}+m_T)}|$ for the applied frequency resolution, and then visually verifying that this is a resonance frequency. The damped non-dimensional eigenfrequency is lower than the undamped non-dimensional eigenfrequency. Roll have an uncoupled eigenfrequency at the non-dimensional squared frequency $\frac{\omega_{n3}^2 R}{g} = 1.42$. The uncoupled and undamped non-dimensional eigenfrequency can be estimated as:

$$\frac{\omega_{n3}^2 R}{g} = \frac{c_{33}R}{g(a_{33}+I_{33})} = 1.42. \tag{64}$$

Since both sides of (64) are dependent on the frequency, the eigenfrequency have been found by finding the first minimum of $|\frac{\omega_{n3}^2 R}{g} - \frac{c_{33}R}{g(a_{33}+I_{33})}|$ for the applied frequency resolution, and then visually verifying that this is a resonance frequency. The estimated uncoupled frequency with and without damping is approximately equal. The coupled rigid body roll–sway response do not have any resonance. The undamped coupled eigenfrequency can be found by considering

$$\frac{\omega_{n3*}^2 R}{g} = \frac{c_{33}a_{11}R}{g((a_{33}+I_{33})a_{11} - a_{13}a_{31})}.$$

No eigenfrequencies can be found from this relation within the considered non-dimensional frequency squared range. This is consistent with Fig. 5, where no resonances were observed.

3.3. Wave induced response of the CFFC including the effect of membrane deformations

Now the response of the CFFC accounting for the flexibility of the 2D membrane will be considered. The transfer functions and phase for the rigid body motions in sway, heave and roll of the CFFC with the flexible membrane are plotted in Fig. 5 and the phase of the motion relative to the incoming wave in Fig. 6. From these figures we observe a large change in both transfer functions of the rigid body motions in sway, heave and roll and in the phase of the coupled response of the CFFC compared to the response of the rigid CFFC.

The transfer functions for the first ten normal and tangential structural modes are plotted in Fig. 7 together with the phase of the motion in Fig. 8 for normal modes and Fig. 9 for tangential modes. From the equations for a half circular membrane (B.3) and (B.4) we observe that there is a coupling between symmetrical normal structural modes and antisymmetrical tangential structural modes, and between antisymmetrical normal structural modes and symmetrical tangential structural modes. This can also be seen in Fig. 7. Hydrodynamically the symmetrical normal membrane modes are coupled with heave and the antisymmetrical normal membrane modes are coupled with sway and roll.

When a deformable membrane is accounted for, Fig. 5 shows that the resonance in heave has disappeared and that the asymptote when ω goes to zero of the heave response have significantly decreased. These are both surprising results. The disappearance of the heave resonance are due to that the coupled system no longer have an eigenfrequency within the given frequency range. The change in asymptote can be explained if we consider (19) when ω goes to zero. We should recall that for symmetric structural normal modes additional stiffness exist from the internal added mass, since $\omega^2 a_{kj}^{(i)} = c_{kj}^{(i)}$ is constant at $\omega \to 0$. If we look at the heave part of (19) for $\omega = 0$

$$c_{22}\xi_2 + \underbrace{\sum_{j=4}^{\infty} c_{2j}^{(i)}\xi_j}_{(1^*)} + \underbrace{\sum_{n=1} c_{2n}^{M\xi\mu}\mu_n}_{(2^*)} = f_{2a}^{exc}. \tag{65}$$

To find the asymptote we must find the generalised excitation force when ω goes to zero. For the symmetric structural modes the wave excitation pressure amplitude can be approximated as constant $\rho_w g \zeta_a$ and the generalised wave

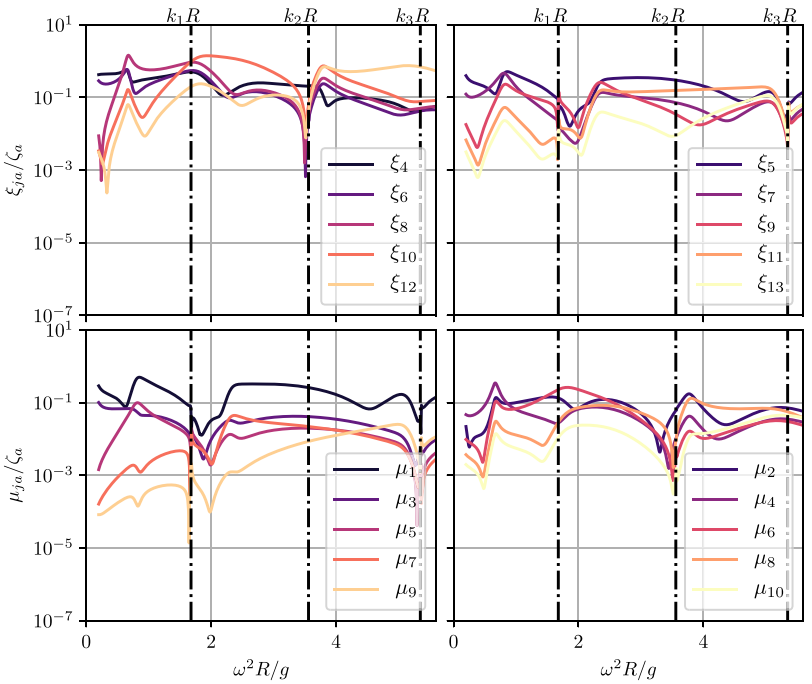

Fig. 7. Transfer functions of normal (top figures) and tangential (bottom figures) structural modes for a CFFC versus non-dimensional squared frequency ω^2R/g, for the first 10 normal and tangential structural modes. Structural damping is 2% of critical damping. k_1R, k_2R and k_3R are non-dimensional natural sloshing frequencies for the CFFC.

excitation force amplitude can be expressed as

$$f_{ja}^{exc} = \rho_w g \zeta_a \int_{S_M} U_{j-3}(\psi_0)\mathrm{ds} = -2\rho_w g \zeta_a R \frac{\sin^2(\pi(j-3)/2)}{j-3} \text{ for } j > 3. \tag{66}$$

The decrease in response at $\omega = 0$ is connected to the coupling to the tangential and normal membrane modes. If (66) is applied to (19) at $\omega = 0$, the asymptote of heave for the coupled case is found to be $\xi_{2a}/\zeta_a = 0.21$. From Fig. 5 we see that the asymptote of heave appears to converge to this value. Physically this can be explained as a reduction in applied force which comes from two spring forces working through the normal and tangential deformations. The spring force from the normal deformation of the membrane (1* in Eq. (65)) lead to a mean elevation of the internal free surface. This rise in the free surface works as a pressure force against the external wave pressure, in total reducing the force on the heave motion. The spring force from the tangential deformations (2* in Eq. (65)) are connected to the dynamic tension in the 2D membrane.

A small amplification of the response of heave can be seen around $\omega^2R/g = 3.71$, close to the second sloshing eigenfrequency. This coincides with the peak in the internal sloshing wave amplitude at this frequency as visible in Fig. 10. An increase can also be seen at this frequency for the symmetrical normal membrane modes in Fig. 7.

From Fig. 5 we see that the asymptote of roll deviates from the rigid body case. Again, this can be explained if we consider (19) when ω goes to zero. If we consider the roll part of (19) for $\omega = 0$

$$c_{33}\xi_3 - \omega^2 a_{31}\xi_1 + \sum_{j=4}^{\infty} c_{3j}^{M\xi}\xi_j + \sum_{n=1} c_{3n}^{M\xi\mu}\mu_n = f_{3a}^{exc}. \tag{67}$$

Roll would be coupled to the asymmetric normal structural modes and the symmetric tangential modes. For the asymmetric normal structural modes the largest wave excitation amplitude for a given time instance when ω goes to zero can be approximated as constant $\rho_w g \zeta_a k y$. For a half circular geometry, $y = R\sin\psi_0$. The generalised wave excitation force amplitude at $\omega = 0$ can then be approximated as

$$f_{ja}^{exc} = \rho_w g \zeta_a k \int_{S_M} R\sin\psi_0 U_{j-3}(\psi_0)\mathrm{ds} = -\rho_w g \zeta_a k R^2 \frac{1+(-1)^{j-3}}{(j-3)^2-1} \text{ for } j > 3. \tag{68}$$

The increase in roll asymptote can be explained through the coupling with the normal and tangential membrane modes. The normal and tangential coupling modes part of (67) will lead to an increase in the load, for positive μ_k and ξ_j for $j > 3$, since $c_{3n}^{M\xi\mu}$ and $c_{3j}^{M\xi}$ are negative (see Appendix B). From Fig. 7 it appears that both μ_k for symmetric tangential modes and

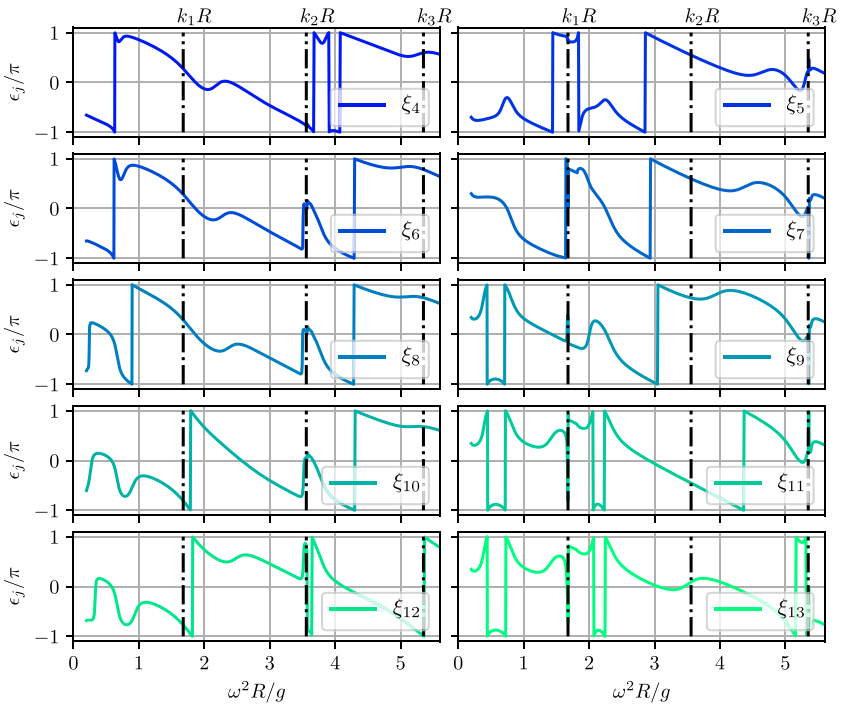

Fig. 8. Phase of normal structural modes for a CFFC versus non-dimensional squared frequency ω^2R/g. For the first 10 normal modes. Structural damping 2% of critical damping. k_1R, k_2R and k_3R are non-dimensional sloshing frequencies for the CFFC.

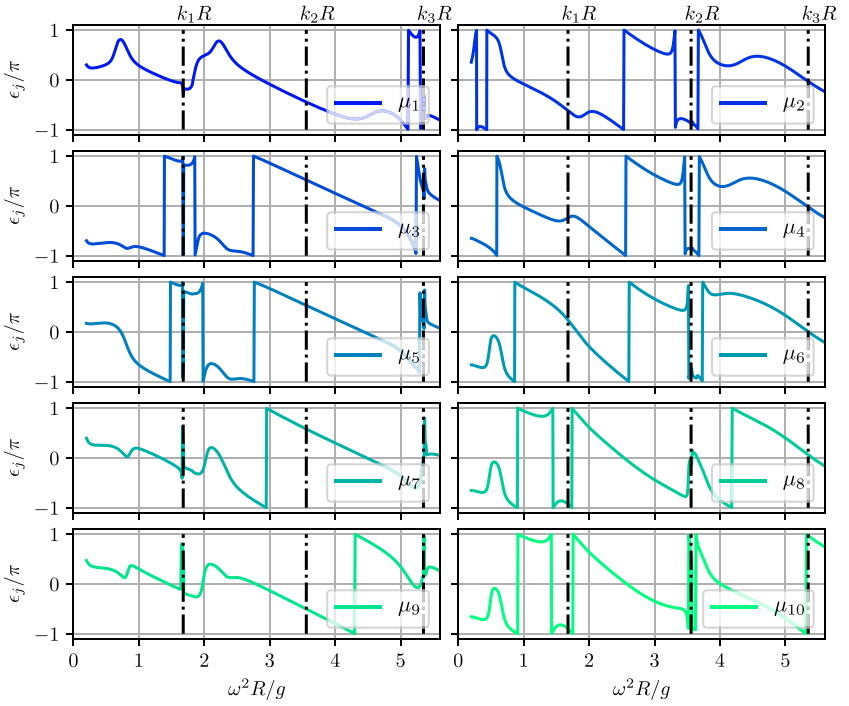

Fig. 9. Phase of tangential structural modes for a CFFC versus non-dimensional squared frequency ω^2R/g. For the first 10 normal modes. Structural damping 2% of critical damping.k_1R, k_2R and k_3R are non-dimensional sloshing frequencies for the CFFC.

ξ_j for $j > 3$ for asymmetric normal modes converge to a constant value for $\omega = 0$. If (68) is applied to (19) at $\omega = 0$, the asymptote of roll for the coupled case is found to be $\xi_{3a}/\zeta_a = 6.33$. This is significantly larger than the rigid response. Also

for roll can the change in load be explained physically with drawing a parallel to a spring, but here the force increases due to spring moments caused by the static tension and the dynamic tension.

The response of sway and roll rapidly decreases to a small value in a narrow frequency range around k_1R and k_3R, as can be seen from Fig. 5. This is different from the coupled response of the rigid CFFC where it was found that this cancellation did not happen. From Fig. 7 we see that the asymmetric normal structural modes have a smaller response at the first and third sloshing eigenfrequency, while the symmetric normal structural modes have a smaller response at the second sloshing eigenfrequency. At the sloshing frequencies the generalised internal added mass approaches infinity, and a small motion response is therefore plausible. A clear shift in phase at the first and third sloshing eigenfrequency response for sway and roll can also be observed from Fig. 6.

All the phases of the normal structural modes have a shift in response at the sloshing frequencies. The phases of the symmetric modes at the second sloshing eigenfrequency and the phases of the antisymmetric modes at the first and third sloshing eigenfrequency. From Fig. 7 we see that the asymmetric normal structural modes have a smaller response at the first and third sloshing eigenfrequency, while the symmetric normal structural modes have a smaller response at the second sloshing eigenfrequency. At the sloshing frequencies the generalised internal added mass approaches infinity, and a small response is therefore plausible.

Considering (B.1) and (B.2) it should be expected that the deformation of the membrane goes to zero when T_0 goes to infinity, and thereby that the response of the coupled system goes to the response of the rigid body system. For heave the system will approach the rigid body solution when the tension approaches infinity. For roll and sway, this is not the case. The reason why the response for roll and sway does not approach the rigid response is that the response is dependent on the static tension multiplied with the dynamic angle. When the static tension approaches infinity, bending will not be negligible at the attachment point between the membrane and the floater. This have not been accounted for in the structural response described by (14) and (15). If bending is accounted for, the dynamic angle will go to zero and the response of the coupled system will also for roll and sway be the response of a rigid body. That T_0 goes to infinity is not a physical case since the tension is dependent on the overfilling Δh, and Δh cannot physically go to infinity. However, it is a good check on the asymptotic behaviour of the structural equations.

The structural convergence related to the number of structural modes in normal and tangential direction have been investigated, by looking at the convergence of the transfer function of the coupled rigid body motions. It have been found that 30 normal and 250 tangential modes are sufficient. The number of tangential modes converges slowly, this can mainly be explained by the low level of structural damping. Compared to the normal structural modes that have both wave radiation damping and higher structural damping due to the influence of the added mass on the structure, the damping level of the tangential modes are small. The wave radiation damping decreases for increasing frequency and both the wave radiation damping and added mass decrease with increasing mode number, but even for the highest modes the normal modes have a higher damping. The number of normal structural modes converges faster. This is probably due to the higher level of damping. The maximum number of normal modes that have been run is 30. The normal structural modes give a hydrodynamic pressure load contribution which must be found from the HPC potential flow solver. It is computationally expensive to add a large number of normal structural modes, because the highest structural mode must be sufficiently resolved in the grid, and that requires a finer grid.

3.4. Internal wave amplitude

Both from a structural load perspective and from a fish health perspective it is interesting to look at the internal wave amplitude inside the cage. A hypothesis during the work was that the membrane causing wave radiation damping would have less sloshing than a rigid tank, because the membrane deformations would work as a damper on the sloshing. That did not appear to happen. The transfer functions of the internal wave amplitude and phase at the right floater and at the centre of the CFFC are plotted in Fig. 10 for both the rigid and deformable membranes. For the internal wave amplitude and the phase at the right floater the response appears to go to infinity at the first and third natural sloshing frequency both for the rigid membrane and for the deformable membrane. The latter natural frequency have a negligible influence of the deformable membrane for the considered static membrane tension. Contrary to our hypothesis of less internal waves for the flexible membrane an additional resonance/ amplification by the second sloshing frequency were observed, where there were no pronounced response for the rigid case. The wave mode at this frequency have a top both by the right floater and at the centre of the CFFC. In total it appears that external wave radiation damping does not appear to affect the results at the first and third sloshing eigenfrequency. However, the exact sloshing eigenfrequency to the finest precision have not been found, so it is not possible to determine if the response is infinite or just very large. To predict the correct internal wave amplitude close to the first and third sloshing eigenfrequencies a non-linear analysis will be needed for a realistic wave environment.

The spatially averaged internal wave amplitude is consistent with volume conservation according to Eq. (52) and is also plotted in Fig. 10. It represents an accumulated effect of the structural deformation on the internal free surface. We observe that the spatially averaged internal wave amplitude is significant at several frequencies compared to the incident wave amplitude ζ_a. Only the symmetric structural modes will have an accumulated effect of the structural deformation on the internal free surface. And, only the anti-symmetric modes will have a response at the first and third sloshing frequency as can be observed of the normal modes response in Fig. 7 where 5, 7, 9, 11 and 13. The response at the first

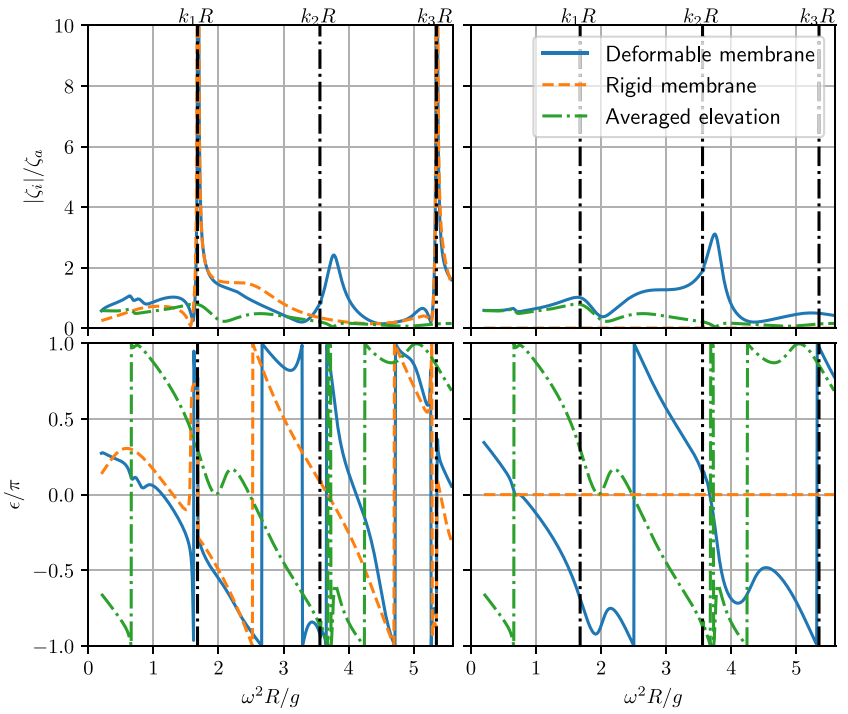

Fig. 10. Top:Transfer functions of the internal wave amplitude at the right floater (left figure) and at the centre (right figure) of the CFFC versus non-dimensional squared frequency ω^2R/g with the effect of the deformable membrane. The space-averaged wave amplitude is also presented. Bottom: Phases of the internal wave amplitude of the CFFC. k_1R, k_2R and k_3R are non-dimensional natural sloshing frequencies for the CFFC.

and third eigenfrequency has therefore not an effect on the average elevation, and the response in the average elevation close to the first eigenfrequency can be attributed to the accumulated large response in the symmetric modes (see Fig. 7). Close to the second eigenfrequency the symmetric normal structural modes have a response, this is however not visible on the average internal wave amplitude which is close to zero, this means that the accumulated deformation of all the modes combined are close to zero. It could appear that the phase have a resonance close to the second sloshing frequency based on the peaks in the phase for the deformable membrane and the averaged elevation, this is not the case. The peaks can be explained by phases crossing back and forth around π.

3.5. Dynamic tension

Within linear membrane theory we must require that the total tension in the membrane at all times is larger than zero, i.e. the dynamic tension τ must be smaller than the static tension T_0. The dynamic tension is dependent on both the wave height and the wave frequency. To find out if the requirement is fulfilled the static tension must be compared to the stochastic amplitude found from relevant sea states.

The results here are based on the full scale values given in Table 1 and for a given overfilling and thereby given static tension T_0. For the calculations of the transfer functions of the dynamic tension τ_a/ζ_a, the tension at the connection point between the membrane and the right floater have been used. The dynamic tension varies along the membrane and the tension at the right floater is not the highest tension for all frequencies. However, for a large part of the frequency range it is the largest dynamic tension or close to largest dynamic tension. It was decided to use the tension at a fixed position on the membrane and the tension at the connection point between the membrane and the right floater was then considered the best choice.

The standard deviation of the dynamic tension σ_τ for a given sea state spectrum $S(\omega)$ in long crested waves can be calculated as:

$$\sigma_\tau^2 = \int_0^\infty S(\omega)\left(\frac{\tau_a}{\zeta_a}\right)^2 \mathrm{d}\omega. \tag{69}$$

The Norwegian standard NS9415 for design of aquaculture fish farm in the sea requires for calculation of response from irregular sea that the JONSWAP spectrum shall be used with $\gamma = 2.5$ for wind-generated seas, where γ is the spectral peakedness parameter. The JONSWAP spectrum is for limited fetch, and in the standard it is required that a fully developed sea state is assumed. A γ value of 2.5 is lower than for ships and offshore structures where $\gamma = 3.3$.

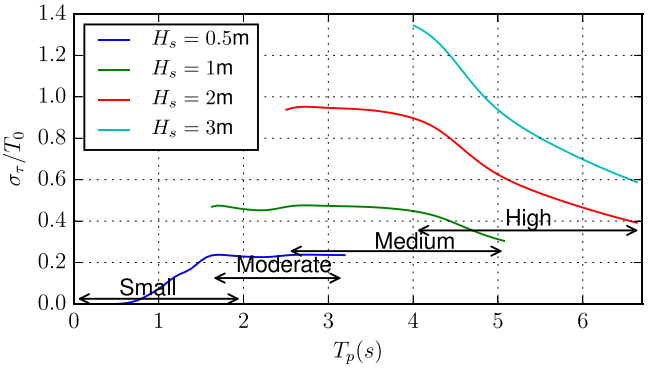

Fig. 11. Non-dimensional dynamic tension variance σ_τ/T_0 for given exposure versus wave peak period T_p in sea states defined by a JONSWAP spectrum. H_s is significant wave height. The small, moderate, medium and high refers the classification related to exposure as given in NS9415.

The JONSWAP spectrum is

$$S(\omega) = \frac{\alpha_p g^2}{\omega^5} \exp\left(\frac{-20\pi^4}{T_p^4 \omega^4}\right) \gamma^{Y_p}, \tag{70}$$

where α_p and Y_p are given as:

$$\alpha_p = \frac{5.061 H_s^2}{T_p^4}(1 - 0.287 \ln \gamma),$$

$$Y_p = \exp\left(-\frac{1}{2}\left(\frac{\frac{\omega T_p}{2\pi} - 1}{\sigma_p}\right)^2\right),$$

with σ_p as the spectral width parameter given as

$$\sigma_p = \begin{cases} 0.07 \text{ for } \omega \leq \frac{2\pi}{T_p} \\ 0.09 \text{ for } \omega > \frac{2\pi}{T_p}. \end{cases}$$

The non-dimensional standard deviation σ_τ/T_0 of the dynamic tension versus wave peak period T_p for given significant wave heights are plotted in Fig. 11. The peak periods T_p and significant wave heights are related to the classification of exposure as given in NS9415. From Fig. 11 we see that σ_τ exceeds T_0 for $H_s = 3$ m for high exposure. If we assume a Rayleigh distribution, the most probable largest value for τ is approximately $4\sigma_\tau$ in a sea state of common duration. $4\sigma_\tau$ exceeds T_0 for all H_s except $H_s = 0.5$m. That the most probable largest value of τ is exceeded for H_s larger than 0.5 m at small exposure is critical, and indicates that other structural models should be used such as including bending stiffness and non-linear stress–strain relations. Furthermore, zero tension could lead to snap loads in the material that could contribute to fatigue. The analysed CFFC is a small cage if the radius R of the cage is compared to industry sizes of aquaculture net cages presently used in Norway.

3.6. Model test scaling

Model scale experiments are often used to gain knowledge of the physics of a new system and to validate numerical models. It is difficult to do 2D experiments to validate the results in this paper. This remains as a further task. However, the present theoretical model provides important information about scaling of model test results for the considered membrane structure. For the model to represent the full scale structure in waves we require Froude scaling which implies that $\omega\sqrt{\frac{R}{g}}$ is equal in model and full scale. If (B.1) and (B.2) are made non-dimensional by $\rho_w g R$, the Froude scale leads to that the non-dimensional parameter $\frac{Ed}{\rho_w g R^2}$ should be the same in model and full scale. Since the gravity g is constant and the water density ρ_w is close to constant, the only values the can be adjusted to meet this condition are the elasticity module and the thickness of the fabric. In the real world this material does not exist for normal model scales. If we use plausible model scale of $1:12.5$ and use the model scale values for the thickness of the fabric $d = 5 \cdot 10^{-5}$ m and the elasticity modulus of nylon $E = 2 \cdot 10^9$ Pa as used in Strand et al. (2016) and Lader et al. (2017), we consider a material that is approximately ten times too stiff for the scale. And, if a larger scale is considered for the radius of the cage, the deviation between the sought material stiffness and the used material stiffness becomes even larger. What effect will this deviation in elasticity have on the results?

The system described in this paper is used to evaluate the effect this "elasticity-error" on the response of the system. The 2D results are not directly comparable, but can give an indication if there is a challenge. The rigid body response of the

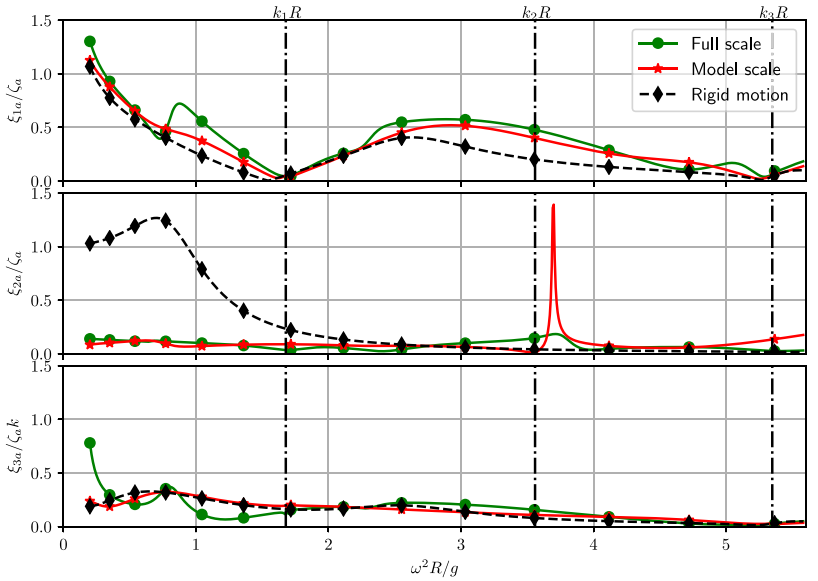

Fig. 12. Transfer functions of motion of a CFFC with deformable membrane for sway (top), heave (middle) and roll (bottom) versus nondimensional frequency $\omega^2 R/g$, for an elasticity modulus used in model experiments and for an elasticity modulus used in full scale. k_1R, k_2R and k_3R are non-dimensional natural sloshing frequencies for the CFFC.

CFFC both for a stiffness used in full scale and the stiffness used in model scale are plotted in Fig. 12. The response of the rigid CFFC in model and full scale is equal, but the coupled system response including the flexible modes deviate to a large extent. This raises severe questions of the use of direct scaling of the results from model experiments for these flexible structures. The model scale results should not be scaled and used directly as the "truth" for full scale cases. However, this does not mean that model scale experiments are useless for validation. The results should be used to validate a numerical model using the model scale stiffness and then the numerical model with the full scale stiffness can be used to predict the full scale values.

4. Conclusions

In this paper the linear theory of a 2D closed flexible fish cage in waves was developed and analysed with the aim to find the response of the CFFC in waves. The results from a 2D case study with relevant full scale dimensions, considering a half circularly shaped CFFC with floaters were presented. Investigations only consider the 2D case. However, the findings can be considered a starting point for analysing 3D structures.

We observe a large change in response of the rigid body motions in sway, heave and roll of the CFFC with deformable membrane compared to the response of the rigid CFFC. The resonance in heave for the rigid CFFC has disappeared and the asymptote when the forcing frequency ω goes to zero of the heave response have significantly decreased. The response of sway and roll rapidly decreases to a small value in a narrow frequency range around the non-dimensional sloshing eigenfrequencies k_1R and k_3R. This is different from the coupled response of the rigid CFFC where it was found that this cancellation did not happen. For a rigid CFFC, uncoupled sway and roll have cancellation at the first and third sloshing frequency. For the CFFC with deformable membrane in coupled sway and roll, no cancellation of the response appears at the first and third sloshing frequency.

The sloshing wave amplitudes of the coupled system are comparable to the sloshing wave amplitudes of the rigid system, for most non-dimensional frequencies and the maximum values occurs typically by the floater. However, a non-negligible sloshing wave amplitude response can also be seen at the centre of the CFFC with deformable membrane at frequencies slightly higher than the second sloshing frequency, which is not present for the rigid body CFFC. Very large ratios between free-surface elevation amplitudes and incident wave amplitude are predicted inside the tank at the first and third natural sloshing frequencies. It implies that non-linear free surface effects must be accounted for inside the tank in realistic sea conditions, as well known from other marine sloshing applications (Faltinsen and Timokha, 2009).

Within linear structural theory we required that the dynamic tension was smaller than the static tension. For the analysed geometry with 25 m between the centre of the floaters, the most probable largest dynamic tension was larger than the static tension, for significant wave heights larger than 0.5 meter. For negative total tensions the structural model is not valid.

The effect of scaling of elasticity on the rigid body motion was also investigated. To scale the results correctly it requires that the elasticity of the membrane material should scale as the diameter, this is unfortunately not straight forward. The

response of the CFFC using an elasticity available in model scale have been compared to the response of the CFFC using the elasticity for full scale. These responses where found to deviate to a large extent. This raises severe questions of the direct use of results from model scale experiments for the CFFC.

Future work should include experimental validation. The described methodology should be generalised to a 3D CFFC with axially symmetric bag at rest. The static analysis can be pursued based on equations in Irvine (1981). The linear potential flow calculations can be performed by a state-of-the-art method that considers membrane deformations. Since the total tension can easily become zero in realistic sea conditions, effects such as bending stiffness and stress–strain non-linearities should be studied. Structural damping for realistic membrane materials must be investigated. A further step would also be to account for non-linear sloshing, which can lead to swirling and chaos. Since a CFD method is time consuming and viscous effects play a secondary role as long as wave breaking does not occur, the nonlinear multimodal method for potential sloshing flow of an incompressible liquid as described by Faltinsen and Timokha (2009) should be attempted. An additional advantage of the multimodal method is explicit acceleration dependent loads that stabilises numerical time integration in wave–body interaction analysis. A CFFC with a mooring system should also be studied. A second-order time domain analysis of the effect of external flow on the hydrodynamic loads on a CFFC must then be included. We also need to study the combined effect of waves and current. The described methodology applies then as long as flow separation does not occur. The importance of viscous flow caused by internal pumps and pipes should be assessed.

Acknowledgements

This work have been financed by the Research Council of Norway through the project "External Sea Loads and Internal Hydraulics of Closed Flexible Cages" (grant no. 216127) and through the project "Safe operation of closed aquaculture cages in waves" (grant no. 268402). The work has been carried out at the Centre for Autonomous Marine Operations and Systems (AMOS), supported by the Research Council of Norway through the Centres of Excellence funding scheme, project number 223254 - AMOS. The Norwegian Research Council is acknowledged as the main sponsor of AMOS.

Appendix A. Relations for structural stiffness coefficients

The structural stiffness coefficients of the normal deformation modes $c_{ij}^{M\xi}$, the structural stiffness coefficients of the tangential deformation modes $c_{kn}^{M\mu}$ the coupling stiffness coefficient between ξ and μ; $c_{in}^{M\xi\mu}$, and the coupling stiffness coefficients between μ and ξ; $c_{kj}^{M\mu\xi}$, are defined according to:

$$c_{ij}^{M\xi} = \int_{S_M} \left(EdU_i \frac{d\psi_0}{ds} - T_0 \frac{d^2U_i}{ds^2} - \frac{dT_0}{ds}\frac{dU_i}{ds} - m_M g \sin\psi_0 \frac{dU_i}{ds} \right) U_{(j-3)} \mathrm{ds} \text{ for } j, i > 3,$$

$$c_{kn}^{M\mu} = \int_{S_M} \left(-Ed\frac{d^2U_k}{ds^2} + T_0 \frac{d\psi_0}{ds}\frac{d\psi_0}{ds} U_k - m_M g \cos\psi_0 U_k \frac{d\psi_0}{ds} \right) U_n \mathrm{ds},$$

$$c_{in}^{M\xi\mu} = \int_{S_M} \left(-Ed\frac{dU_n}{ds} - T_0\left(\frac{dU_n}{ds}\frac{d\psi_0}{ds} + U_n\frac{d^2\psi_0}{ds^2}\right) - \frac{dT_0}{ds}U_n\frac{d\psi_0}{ds} - m_M g \sin\psi_0 U_n \frac{d\psi_0}{ds} \right) U_{(i-3)} \mathrm{ds} \text{ for } i > 3$$

$$c_{kj}^{M\mu\xi} = \int_{S_M} \left(Ed\left(\frac{dU_{(j-3)}}{ds}\frac{d\psi_0}{ds} + U_{(j-3)}\frac{d^2\psi_0}{ds^2}\right) + T_0\frac{d\psi_0}{ds}\frac{dU_{(j-3)}}{ds} - m_M g \cos\psi_0 \frac{dU_{(j-3)}}{ds} \right) U_k \mathrm{ds}.$$

$c_{ij}^{M\xi}$ and $c_{in}^{M\xi\mu}$ for $i < 4, j > 3$ are defined by (24).

Appendix B. Membrane equation system for the membrane deformations for a semi-circular membrane

A case where the static membrane geometry is half circular is analysed. For the shape to be fully half circular the static tension must be much larger than the mass forces on the 2D membrane, i.e $T_0 \gg \pi R m_M g$, then the static tension variations along the membrane $\partial T_0/\partial s = 0$, and the mass terms can be neglected. For a half circular membrane, the static curvature is constant, then $\frac{\partial\psi_0}{\partial s} = \frac{1}{R}$.

For the given problem the equations simplifies to:

$$-\omega^2 m_M v = \frac{T_0}{R^2}\left(\frac{\partial^2 v}{\partial\psi^2} + \frac{\partial u}{\partial\psi}\right) + \frac{Ed}{R^2}\left(\frac{\partial u}{\partial\psi} - v\right) - \Delta\hat{p} \tag{B.1}$$

$$-\omega^2 m_M u = \frac{Ed}{R^2}\left(\frac{\partial^2 u}{\partial\psi^2} - \frac{\partial v}{\partial\psi}\right) - \frac{T_0}{R^2}\left(\frac{\partial v}{\partial\psi} + u\right) \tag{B.2}$$

The rigid body equation of motion given by (1)–(3) and the equations for the structural deformations of the membrane by (B.1) and (B.2) combined with (16) and (17), multiplied with the mode and integrated along the membrane, together

give a representation of the dynamics of the CFFC. For a half circular shape $\psi_e = \pi/2$. $U_j(\psi_0) = \sin(j(\psi_0 - \frac{\pi}{2}))$. By using orthogonal properties, the resulting equation system become:

$$\sum_{j=1}^{\infty}\left(-\omega^2(m_{ij}^{\xi} + a_{ij}) + \mathrm{i}\omega b_{ij} + c_{ij} + c_{ij}^{M\xi}\right)\xi_j + \sum_{n=1}^{\infty} c_{in}^{M\xi\mu}\mu_n = f_i^{exc} \text{ for } i = 1....\infty \tag{B.3}$$

$$\left(-\omega^2 m_{kk}^{\mu} + c_{kk}^{M\mu}\right)\mu_k + \sum_{j=1}^{\infty} c_{kj}^{M\mu\xi}\xi_n = 0 \text{ for } k = 1....\infty \tag{B.4}$$

Here, the non-zero m_{ij}^{ξ} for $i, j < 4$ follow from (1)–(3) and are $m_{11}^{\xi} = m_{22}^{\xi} = m_T$, $m_{33}^{\xi} = I_{33}$ and $m_{13}^{\xi} = m_{31}^{\xi} = -z_G m_T$. The non-zero generalised mass coefficients m_{ii}^{ξ} for $i > 3$ and m_{kk}^{μ} associated with the normal and tangential deformation modes are given as $m_{ii}^{\xi} = m_{kk}^{\mu} = m_M R\frac{\pi}{2}$. The expressions for the structural stiffness coefficients can be calculated as $c_{ii}^{M\xi} = \frac{\pi(Ed+(i-3)^2 T_0)}{2R}$ for $i > 3$ and $c_{nn}^{M\mu} = \frac{\pi(n^2 Ed+T_0)}{2R}$. Due to orthogonal properties are $c_{ik}^{M\xi} = c_{ik}^{M\mu} = 0$ for $i > 3$ and $i \neq k$. The structural stiffness coefficients from the tension forces on the floaters from the membrane are $c_{ij}^{M\xi} = [-\frac{T_0}{R}(j-3)((-1)^{(j-3)}+1), 0, z_e^2\frac{T_0}{R}(j-3)((-1)^{(j-3)}+1)]^T$ and $c_{in}^{M\xi\mu} = [0, -Edn((-1)^n+1), -R^2 Edn((-1)^n-1)]^T$ for $i = 1, 2, 3$. The expressions for the coupled membrane structural stiffness coefficients are $c_{in}^{M\xi\mu} = -\frac{\pi(Ed+T_0)}{2R} n\alpha_{(i-3)n}$ and $c_{kj}^{M\mu\xi} = \frac{\pi(Ed+T_0)}{2R}(j-3)\alpha_{k(j-3)}$ for $i > 3$, where α_{jm} is defined according to:

$$\int_{-\pi}^{0} U_{cm}(\psi_0)U_j(\psi_0)d\psi = \alpha_{jm} = \begin{cases} 0 \text{ for } m = j \\ \frac{j((-1)^j(-1)^m-1)}{j^2-m^2} \text{ for } m \neq j \end{cases} \tag{B.5}$$

where $U_{cj}(\psi_0)$ comes from the first derivative of $U_j(\psi_0)$ and is defined as $U_{cj}(\psi_0) = \cos(j(\psi_0 - \frac{\pi}{2}))$. Symmetry properties can be observed from the α_{jm} expressions defined in (B.5). Symmetric normal membrane modes are structurally coupled to antisymmetric tangential membrane modes and antisymmetric normal membrane modes are coupled to symmetric tangential membrane modes.

Appendix C. Formulations of the numerical potential theory harmonic polynomial cell (HPC) method

The basic formulation of the HPC method is based on (Shao and Faltinsen, 2014a). A local Cartesian x, y coordinates system is used and the domain is divided into cells with nine nodes. The velocity potential in each cell is described by an interpolation function

$$\phi(x, y) = \sum_{j=1}^{8} b_j f_j(x, y) \tag{C.1}$$

where b_j and $f_j(x, y)$ are coefficients and harmonic polynomials respectively. The harmonic polynomial automatically satisfies the Laplace equation ($\nabla^2\phi = 0$) everywhere in space.

The Harmonic Polynomials are chosen as follows:

$$\begin{aligned} F(x, y) &= [f_1(x, y), f_2(x, y), f_3(x, y), f_4(x, y), f_5(x, y), f_6(x, y), f_7(x, y), f_8(x, y)] \\ &= [1,\ x,\ y,\ x^2 - y^2,\ 2xy,\ x^3 - 3xy^2,\ 3x^2y - y^3,\ x^4 - 6x^2y^2 + y^4\ ] \end{aligned} \tag{C.2}$$

By calculating the velocity potential for nodes 1–8 we get an equation system on the form of

$$\begin{bmatrix} \phi_1 \\ \vdots \\ \phi_8 \end{bmatrix} = \begin{bmatrix} f_1(x_1, y_1)\ldots f_8(x_1, y_1) \\ \vdots\ddots\vdots \\ f_1(x_8, y_8)\ldots f_8(x_8, y_8) \end{bmatrix} \begin{bmatrix} b_1 \\ \vdots \\ b_8 \end{bmatrix} \tag{C.3}$$

Where x, and y is given in local coordinates calculated with centre in node 9.

If (C.3) is solved for b_j we get an expression for the unknown coefficients, given according to

$$\begin{bmatrix} b_1 \\ \vdots \\ b_8 \end{bmatrix} = \underbrace{\begin{bmatrix} f_1(x_1, y_1)\ldots f_8(x_1, y_1) \\ \vdots\ddots\vdots \\ f_1(x_8, y_8)\ldots f_8(x_8, y_8) \end{bmatrix}^{-1}}_{C} \begin{bmatrix} \phi_1 \\ \vdots \\ \phi_8 \end{bmatrix} = \begin{bmatrix} c_{1,1}\ldots c_{1,8} \\ \vdots\ddots\vdots \\ c_{8,1}\ldots c_{8,8} \end{bmatrix} \begin{bmatrix} \phi_1 \\ \vdots \\ \phi_8 \end{bmatrix} \tag{C.4}$$

The resulting velocity potential in the cell can be found from the previous equations according to:

$$\phi(x, y) = \sum_{j=1}^{8} b_j f_j(x, y) = \sum_{i=1}^{8}\left[\sum_{j=1}^{8} c_{j,i} f_j(x, y)\right]\phi_i \tag{C.5}$$

Eqs. (C.2)–(C.5) are given for the local coordinate system (x, y). We choose this coordinate system such that node 9 is located at the origin. This gives a governing relation for the internal nodes in the internal domain, according to

$$\phi(x_9, y_9) = \phi_9 = \sum_{i=1}^{8} c_{1,i}\phi_i \tag{C.6}$$

For nodes at the boundary of the domain the Neumann and Dirichlet boundary conditions are given according to:

$$\frac{\partial \phi}{\partial n} = \sum_{i=1}^{8}\left[\sum_{j=1}^{8} c_{j,i}\nabla f_j(x, y)\cdot \vec{n}(x, y)\right]\phi_i \tag{C.7}$$

$$\phi^* = \phi(x, y) \tag{C.8}$$

where ϕ^* is a known solution and $\vec{n}(x, y)$ is the normal vector at x, y.

A global matrix system is established by inserting the local matrix equations and boundary conditions into the global coefficient matrix, given as:

$$\mathbf{A}_G\boldsymbol{\phi}_G = \mathbf{B}_G \tag{C.9}$$

where $\mathbf{A}_G$ is the global coefficient matrix, $\boldsymbol{\phi}_G$ is the global velocity potential vector and $\mathbf{B}_G$ is the boundary condition vector.

References

Bai, K.J., Yeung, R.W., 1974. Numerical solutions to free-surface flow problems. In: 10th Symposium on Naval Hydrodynamics: Hydrodynamics for Safety, Fundamental Hydrodynamics. Cambridge, Mass., June 24–28, 1974. U.S. Government Printing Office.

Billingham, J., King, A., 2009. Wave Motion (Cambridge Texts in Applied Mathematics). Cambridge: Cambridge Unviersity Press.

Bliek, A., 1984. Dynamic Analysis of Single Span Cables. Massachusetts Institute of Technology, Trondheim.

Faltinsen, O.M., 1990. Sea Loads on Ships and Offshore Structures. Cambridge University Press.

Faltinsen, O.M., 2005. Hydrodynamics of High-speed Marine Vehicles. Cambridge University Press, Cambridge.

Faltinsen, O.M., Timokha, A.N., 2009. Sloshing. Cambridge.

Hanssen, F.-C.W., Bardazzi, A., Lugni, C., Greco, M., 2017. Free-surface tracking in 2D with the harmonic polynomial cell method: Two alternative strategies. Internat. J. Numer. Methods Engrg..

Hanssen, F.W., Greco, M., Shao, Y., 2015. The harmonic polynomial cell method for moving bodies immersed in a Cartesian background grid. In: ASME. International Conference on Offshore Mechanics and Arctic Engineering. In: Prof. Robert F Beck Honoring Symposium on Marine Hydrodynamics, vol. 11, http://dx.doi.org/10.1115/OMAE2015-41282.

Hawthorne, W.R., 1961. The early development of the Dracone flexible barge. Proc. Inst. Mech. Eng. 1847–1982.

Irvine, M.H., 1981. Cable Structures, first ed. The MIT Press, Cambridge, Mass.

Kreyszig, E., Kreyszig, H., Norminton, E.J., 2006. Advanced Engineering Mathematics. Wiley, Hoboken, N.J..

Kristiansen, T., Faltinsen, O.M., 2012. Modelling of current loads on aquaculture net cages. J. Fluids Struct. 34, 218–235. http://dx.doi.org/10.1016/j.jfluidstructs.2012.04.001.

Kristiansen, T., Faltinsen, O.M., 2015. Experimental and numerical study of an aquaculture net cage with floater in waves and current. J. Fluids Struct. 54, 1–26. http://dx.doi.org/10.1016/j.jfluidstructs.2014.08.015.

Lader, P., Fredriksson, D.W., Volent, Z., DeCew, J., Rosten, T., Strand, I.M., 2015. Drag forces on, and deformation of, closed flexible bags. J. Offshore Mech. Arct. Eng. 137 (August), 041202. http://dx.doi.org/10.1115/1.4030629.

Lader, P., Fredriksson, D.W., Volent, Z., DeCew, J., Rosten, T., Strand, I.M., 2017. Wave response of closed flexible bags. J. Offshore Mech. Arct. Eng. 139 (5), http://dx.doi.org/10.1115/OMAE2016-54146.

Løland, G., Aarsnes, J.V., 1994. Fabric as construction material for marine applications. In: Hydroelasticity in Marine Technology. pp. 275–286.

Ma, S., Hanssen, F.-C.W., Siddiqui, M.A., Greco, M., Faltinsen, O.M., 2017. Local and global properties of the harmonic polynomial cell method: In-depth analysis in two dimensions. Internat. J. Numer. Methods Engrg. http://dx.doi.org/10.1002/nme.5631.

Malenica, S., Molin, B., Tuitman, J.T., Bigot, F., Senjanovic, I., 2009. Some aspects of hydrostatic restoring for elastic bodies. In: Abstract for 24th IWWWFB, Saint Petersbourg, Russia, 2009.

Malenica, S., Vladimir, N., Choi, Y.M., Senjanovic, I., Kwon, S.H., 2015. Global hydroelastic model for liquid cargo ships. In: Seventh International Conference on Hydroelasticity in Marine Technology, Split, Croatia, pp. 493–505.

Newman, J.N., 1962. The exciting forces on fixed bodies in waves. J. Ship Res. 6 (4), 10–17.

Newman, J.N., 1994. Wave effects on deformable bodies. Appl. Ocean Res. 16 (1), 47–59. http://dx.doi.org/10.1016/0141-1187(94)90013-2.

Newman, J.N., 2005. Wave effects on vessels with internal tanks, in: 20th Workshop on Water Waves and Floating Bodies - Spitsbergen - 29 May–1 June 2005.

NS9415, 2009. Marine Fish Farms - Requirements for Site Survey, Risk Analyses, Design, Dimensioning, Production, Installation and Operation. Norwegian standard, SN / K 509.

Phadke, A.C., Cheung, K.F., 2001. Resonance and response of fluid-filled membrane in gravity waves. Appl. Ocean Res. 23 (1), 15–28. http://dx.doi.org/10.1016/S0141-1187(00)00026-2.

Quistwater, J.M.R., Dunell, B.A., 1958. Dynamic mechanical properties of nylon 66 and the plasticizing effect of water vapor on nylon. J. Polym. Sci. 28 (117), 309–318. http://dx.doi.org/10.1002/pol.1958.1202811706.

Senjanovic, I., Tomic, M., Tomasevic, S., 2008. An explicit formulation for restoring stiffness and its performance in ship hydroelasticity. Ocean Eng. 35 (13), 1322–1338. http://dx.doi.org/10.1016/j.oceaneng.2008.06.004.

Shao, Y., Faltinsen, O.M., 2014a. Fully-nonlinear wave-current- body interaction analysis by a harmonic polynomial cell method. J. Offshore Mech. Arct. Eng. 136 (August), 8–13. http://dx.doi.org/10.1115/1.4026960.

Shao, Y., Faltinsen, O.M., 2014b. A harmonic polynomial cell (HPC) method for 3D Laplace equation with application in marine hydrodynamics. J. Comput. Phys. 274, 312–332. http://dx.doi.org/10.1016/j.jcp.2014.06.021.

Solaas, F., Rudi, H., Berg, A., Tvinnereim, K., 1993. Floating fish farms with bag pens. In: International Conference on Fish Farming Technology, pp. 317–323.

Strand, I.M., 2018. Sea loads on closed flexible fish cages. In: Doktoravhandlinger ved NTNU, vol. 2018:28, Norwegian University of Science and Technology, Faculty of Engineering, Department of Marine Technology, Trondheim.

Strand, I.M., Faltinsen, O.M., 2017. Linear sloshing in a 2D rectangular tank with a flexible sidewall. J. Fluids Struct. 73, 70–81. http://dx.doi.org/10.1016/j.jfluidstructs.2017.06.005.

Strand, I.M., Sørensen, A.J., Volent, Z., 2014. Closed flexible fish cages: Modelling and control of deformations. In: Proceedings of 33rd International Conference on Ocean, Offshore and Arctic Engineering. June 8–13, 2014, San Francisco, USA, http://dx.doi.org/10.1115/OMAE2014-23059.

Strand, I.M., Sørensen, A.J., Volent, Z., Lader, P., 2016. Experimental study of current forces and deformations on a half ellipsoidal closed flexible fish cage. J. Fluids Struct. vol. 65, http://dx.doi.org/10.1016/j.jfluidstructs.2016.05.011.

Ventsel, E., 2001. Thin Plates and Shells: Theory, Analysis, and Applications. Marcel Decker, New York.

Zhao, R., 1995. A complete linear theory for a two-dimensional floating and liquid-filled membrane structure in waves. J. Fluids Struct. 9 (8), 937–956. http://dx.doi.org/10.1006/jfls.1995.1053.

Zhao, R., Aarsnes, J.V., 1998. Numerical and experimental studies of a floating and liquid-filled membrane structure in waves. Ocean Eng. 25 (9), 753–765. http://dx.doi.org/10.1016/S0029-8018(97)00013-9.

Zhao, R., Triantafyllou, M., 1994. Hydroelastic analyses of a long flexible tube in waves. In: Hydroelasticity in Marine Technology. Trondheim, Norway, pp. 287–300.